

Robust differentiation of human pluripotent stem cells into mural progenitor cells via transient activation of *NKX3.1*

Received: 29 December 2023

Accepted: 13 September 2024

Published online: 30 September 2024

 Check for updates

Umji Lee^{1,2,9}, Yadong Zhang^{3,4,9}, Yonglin Zhu^{1,2}, Allen Chilun Luo¹, Liyan Gong^{1,2}, Daniel M. Tremmel^{1,2}, Yunhye Kim⁵, Victoria Sofia Villarreal¹, Xi Wang⁶, Rwei-Zeng Lin^{1,2}, Miao Cui³, Minglin Ma⁶, Ke Yuan⁵, Kai Wang^{1,2,7}✉, Kaifu Chen^{3,4}✉ & Juan M. Melero-Martin^{1,2,8}✉

Mural cells are central to vascular integrity and function. In this study, we demonstrate the innovative use of the transcription factor *NKX3.1* to guide the differentiation of human induced pluripotent stem cells into mural progenitor cells (iMPCs). By transiently activating *NKX3.1* in mesodermal intermediates, we developed a method that diverges from traditional growth factor-based differentiation techniques. This approach efficiently generates a robust iMPC population capable of maturing into diverse functional mural cell subtypes, including smooth muscle cells and pericytes. These iMPCs exhibit key mural cell functionalities such as contractility, deposition of extracellular matrix, and the ability to support endothelial cell-mediated vascular network formation in vivo. Our study not only underscores the fate-determining significance of *NKX3.1* in mural cell differentiation but also highlights the therapeutic potential of these iMPCs. We envision these insights could pave the way for a broader use of iMPCs in vascular biology and regenerative medicine.

Mural cells, which include pericytes and vascular smooth muscle cells (SMCs), are essential components of blood vessels, playing critical roles in vascular development, stability, and function^{1,2}. Pericytes are primarily associated with microvessels, such as capillaries, while SMCs are more commonly found in larger vessels like arteries and veins³. Mural cells contribute to vessel stabilization, blood flow regulation, endothelial cell quiescence, and the integrity of the blood-brain barrier⁴. However, their dysregulation can lead to vascular abnormalities, including aberrant angiogenesis, vessel destabilization, and impaired vascular function⁵. Consequently, the generation of functional mural cells is essential for understanding vascular function in health and

diseases and for developing novel therapeutic approaches targeting perivascular cells^{2,6}.

The emergence of human induced pluripotent stem cells (hiPSCs) provided a promising and noninvasive approach to obtaining patient-specific mural cells. Conventional methods for mural cell differentiation are largely based on vascular development and involve transitioning hiPSCs through two distinct stages. Initially, hiPSCs are differentiated into intermediate mesodermal progenitor cells (MePCs), regulated by Wnt and/or Nodal signaling pathways. Subsequently, the cells undergo SMC specification, primarily driven by TGF β and PDGF signaling^{7,8}. Despite advancements in chemically induced strategies, there has been growing interest in employing inducible

¹Department of Cardiac Surgery, Boston Children's Hospital, Boston, MA, USA. ²Department of Surgery, Harvard Medical School, Boston, MA, USA.

³Department of Cardiology, Boston Children's Hospital, Boston, MA, USA. ⁴Department of Pediatrics, Harvard Medical School, Boston, MA, USA. ⁵Division of Pulmonary Medicine, Boston Children's Hospital, Boston, MA, USA. ⁶Department of Biological and Environmental Engineering, Cornell University, NY, USA.

⁷Department of Physiology and Pathophysiology, School of Basic Medical Sciences, State Key Laboratory of Vascular Homeostasis and Remodeling, Peking University, Beijing, China. ⁸Harvard Stem Cell Institute, Cambridge, MA, USA. ⁹These authors contributed equally: Umji Lee, Yadong Zhang.

✉ e-mail: kai.wang88@pku.edu.cn; kaifu.chen@childrens.harvard.edu; juan.melero martin@childrens.harvard.edu

transcription factors (TFs) for differentiation⁹. Utilizing TF-based approaches offers several benefits, such as precise temporal control and the possibility of developing methods for the simultaneous differentiation of multiple cell types. However, the identification of a TF that can be effectively leveraged for mural cell differentiation remains elusive.

NK3 Homeobox 1 (NKX3.1) is a TF belonging to the NKX family of homeodomain-containing proteins and plays a pivotal role in the development and maintenance of various tissues, particularly in prostate and SMC differentiation^{10,11}. During SMC differentiation, NKX3.1 interacts with Serum Response Factor (SRF), a critical TF involved in regulating smooth muscle-specific gene expression^{11–13}. Moreover, NKX3.1 cooperates with additional TFs and coactivators, such as GATA-6 and myocardin, further modulating the transcriptional activity of SRF and promoting the expression of smooth muscle-specific genes^{13–15}. Thus, molecular interactions mediated by NKX3.1 collectively contribute to establishing and maintaining the SMC phenotype. Nevertheless, the feasibility of utilizing NKX3.1 as a single fate-determining TF to guide iPSC differentiation into mural cells has not yet been investigated.

Here, we demonstrate that transient activation of NKX3.1 in human MePCs robustly drives their differentiation into progenitor cells capable of contributing to mural cell lineage in their gene expression profiles and functional characteristics. These iPSC-derived mural progenitor cells (iMPCs) are capable of further maturation upon co-culture with endothelial cells (ECs), generating heterogeneous mural cell subpopulations that include pericytes and SMCs. Importantly, iMPCs exhibit robust angiogenic capacity and support EC engraftment in the form of functional vessels *in vivo*, highlighting their therapeutic potential for vascular repair and regenerative medicine applications. Our study establishes NKX3.1 as a key regulator of mural cell differentiation from iPSCs and presents a strategy for generating mural progenitors, opening new avenues for understanding mural cell biology and developing innovative therapeutic approaches for vascular diseases.

Results

NKX3.1 activation efficiently differentiates mesodermal intermediates into mural cells

To evaluate the differentiation potential of NKX3.1, we first genetically engineered human iPSCs to express NKX3.1 in response to doxycycline (Dox) using a piggyBac transposon system. Puromycin-selected clones were screened for homogeneous expression of NKX3.1 upon administration of Dox (Supplementary Fig. 1). The engineered clones (termed iPSC-Dox-NKX3.1) remained pluripotent and maintained the expression of pluripotency markers OCT4, SOX2, and NANOG at comparable levels to the parental iPSC counterpart (Supplementary Fig. 1). Next, we developed a two-dimensional, feeder-free, and chemically defined protocol that relies on a timely transition of iPSCs through two distinct stages, each lasting 48 h (Fig. 1A). The first step entails the conversion of iPSCs into intermediate MePCs, which is mediated by the activation of Wnt signaling pathways using the glycogen synthase kinase 3 inhibitor CHIR99021 and is characterized by the transient activation of the TF TBXT (Supplementary Fig. 6B, D). The second step involves the activation of NKX3.1 for 48 h via the provision of Dox in the absence of any growth factors (Fig. 1B). Thereafter, the resulting cells, herein termed iMPCs, were grown in a serum-containing smooth muscle growth medium (SMGM) for additional passages.

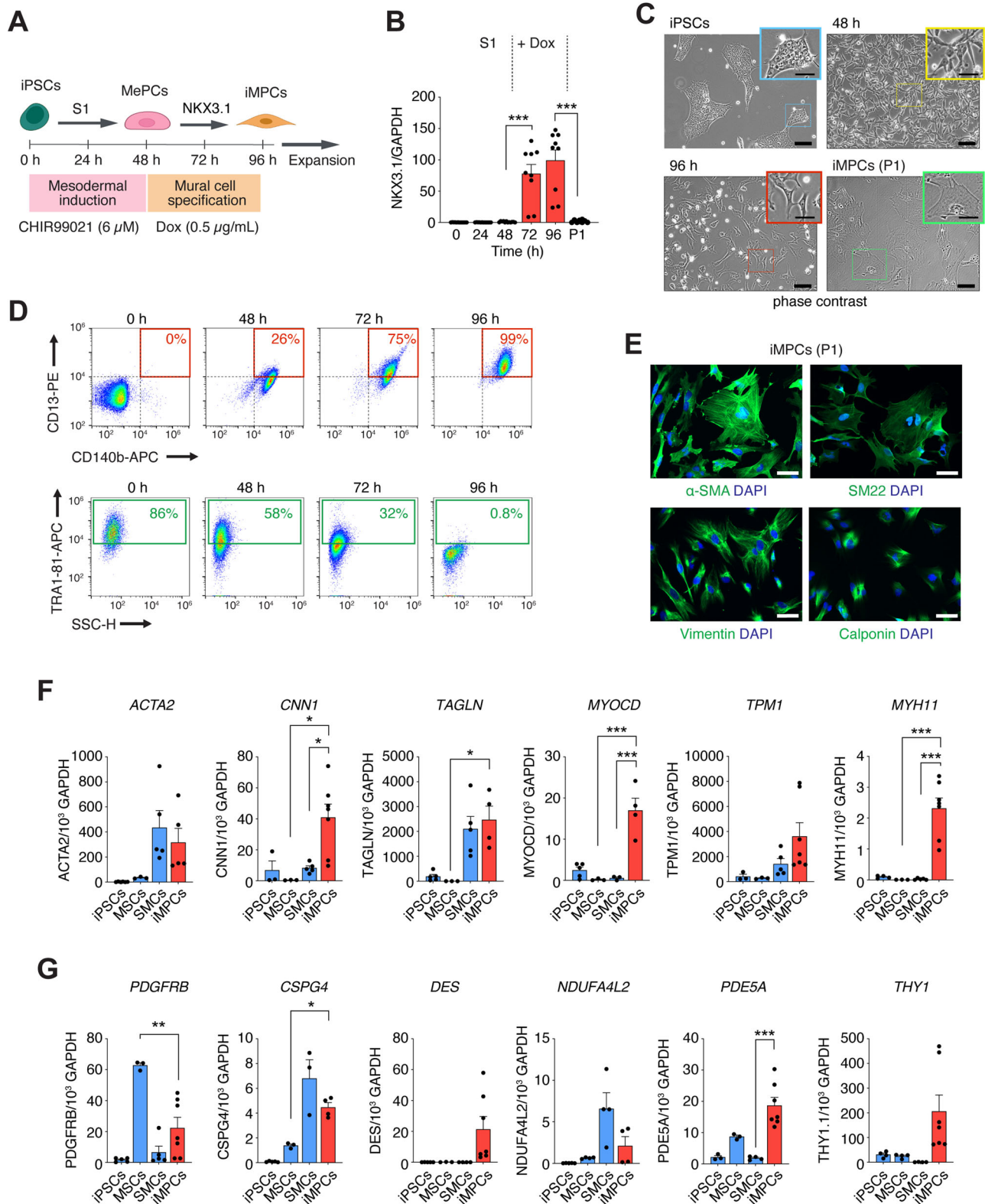
During the 4 days of differentiation, we observed significant morphological changes in the cells that progressively resembled those of mesenchymal cell types (Fig. 1C). Moreover, iMPCs morphologically resembled mural cells in culture, displaying a characteristic stellate shape (Fig. 1C). We traced the presence of mural populations during differentiation using flow cytometry by analyzing the expression of PDGFR β (CD140b), a general mural cell

marker, and aminopeptidase N (CD13), known to be expressed in mural cells *in vivo*¹⁶. Our two-step protocol rapidly and uniformly converted CD140b-/CD13- iPSCs into CD140b+/CD13+ iMPCs with exceedingly high efficiency. Indeed, 48 h after NKX3.1 activation, ~99% of the cells were CD140b+/CD13+ cells (Fig. 1D). Moreover, after 4 days of differentiation, less than 1% of the cells expressed the TRA1-81 antigen, indicating a negligible presence of undifferentiated iPSCs (Fig. 1D). This effective conversion of MePCs into PDGFR β + iMPCs via activation of NKX3.1 was reproducible across iPSC lines from three distinct cellular origins (Supplementary Fig. 3).

After differentiation, indirect immunofluorescence confirmed the expression of mural-specific contractile cytoskeletal proteins in iMPCs, including alpha-smooth muscle actin (α -SMA), calponin, transgelin (SM22), and vimentin (Fig. 1E). The expression of these mural cell markers was highly uniform (>90%) and reproducible across iMPCs derived from three distinct iPSC lines (Supplementary Fig. 4). To further confirm mural cell specification, we compared mRNA expression of iMPCs with those of control human primary pulmonary vascular SMCs and adipose tissue-derived mesenchymal stem cells (MSCs) by qPCR (Fig. 1F, G). The expression of selected smooth muscle markers was either equal to (e.g., *ACTA2*, *TPM1*) or significantly higher (*CNN1*, *TAGLN*, *MYOCD*, *MYH11*) in iMPCs compared to SMCs and MSCs (Fig. 1F). Similarly, the expression of various pericyte markers (*PDGFRB*, *CSPG4*, *DES*, *NDUFA4L2*, *PDE5A*, and *THY1*) was either comparable or significantly upregulated in iMPCs, with the exception of *PDGFRB* expression, which was higher in MSCs (Fig. 1G). Importantly, in the absence of Doxycycline, expression levels of mural cell markers were significantly lower, supporting NKX3.1's role in mural cell specification (Supplementary Fig. 2).

It is important to note that during the differentiation of MePCs to iMPCs, the expression of NKX3.1 was only transient (Figs. 1B and S6). This transitory expression enabled the possibility of using chemically modified mRNA (modRNA), thus developing a genomic footprint-free protocol. Indeed, transfection of unmodified iPSCs with modRNA encoding NKX3.1 enabled robust transient expression of NKX3.1 (Supplementary Fig. 5). Moreover, activation of NKX3.1 with modRNA in MePCs efficiently produced iMPCs that were indistinguishable from those generated by the Dox-inducible protocol, including a robust expression of mural cell markers (Supplementary Fig. 5).

Next, we compared iMPCs generated using our NKX3.1-induced protocol to SMCs derived from iPSCs through a chemically induced approach inspired by a previously reported study⁸. Specifically, these induced SMCs (herein termed iSMCs to be consistent with previous terminology) were generated by exposing MePCs to PDGF-BB (10 ng/mL) and Activin A (2 ng/mL) for 48 h (Supplementary Fig. 6). It is important to note that our protocol for generating iSMCs was inspired by, rather than directly following, the protocol described by Patsch et al.⁸. We adopted only the mesodermal to mural cell differentiation aspects of their protocol (i.e., the use of PDGF-BB and Activin A) to enable a comparable mesodermal stage and effectively compare the outcomes of our NKX3.1 induction protocol with a chemically induced protocol. Cells during both the NKX3.1-induced and chemically-induced protocols exhibited a similar sequential pattern of transient expression of *TBXT* and *NKX3.1*, coinciding with their transition through mesodermal and mural cell differentiation stages, respectively (Supplementary Fig. 6). Both iMPCs and iSMCs consistently expressed SMC markers at similar levels, except for *ACTA2* and *MYOCD*, which were significantly higher in iSMCs (Supplementary Fig. 6). Meanwhile, the expression of pericyte markers was more prevalent in iMPCs than in iSMCs (Supplementary Fig. 6). Of note, both iMPCs and iSMCs exhibited minimal *MYH11* expression (Supplementary Fig. 6), which is consistent with a subdued expression in SMCs expanded in culture¹⁷. Together, these data suggest that while both protocols are



effective at generating mural cells, the chemically-induced method preferentially produces cells consistent with an SMC phenotype, whereas the NKX3.1-induced protocol generates iMPCs with characteristics of both SMCs and pericytes.

In summary, the transient activation of NKX3.1 expression in MePCs (via a Dox-inducible system or modRNA) effectively and efficiently converted human iPSCs into cells exhibiting a distinct mural cell phenotype.

Contractile and secretory competence of iMPCs

Next, we assessed the functional attributes of iMPCs, with a particular focus on characteristics commonly associated with mural cells. Key functions explored included calcium influx, contractile properties, extracellular matrix (ECM) synthesis, and the ability to interact with ECs and maintain vessel integrity in vivo.

We examined the contractility of iMPCs by stimulation with vasoconstrictive agents. Calcium imaging demonstrated that both

Fig. 1 | NKX3.1-induced differentiation of MePCs into iMPCs. **A** Differentiation Schema: Illustration of the stepwise differentiation from iPSCs to iMPCs, detailing mesodermal induction, mural cell specification, and expansion phases. **B** NKX3.1 Expression: Time-course qRT-PCR analysis demonstrating NKX3.1 upregulation during differentiation ($n = 9$; $***P < 0.001$). **C** Morphological Progression: Phase-contrast microscopy revealing morphological evolution at various stages (Scale bars: 100 μm ; insets 50 μm). **D** Flow Cytometry: Analysis of CD13 and CD140b (mural cell markers), and TRAI-81 (pluripotency marker) throughout differentiation stages. **E** Cytoskeletal Markers: Immunofluorescence of iMPCs for α -

SMA, SM22, Vimentin, and Calponin with DAPI nuclear staining (Scale bars: 50 μm). **F** Smooth Muscle Markers: qRT-PCR quantification of SMC gene expression ($n = 3, 4, 5, 7$; $*P < 0.05$, $***P < 0.001$). **G** Pericyte Markers: qRT-PCR analysis showing pericyte-specific gene expression ($n = 3, 4, 5, 7$; $*P < 0.05$, $**P < 0.01$, $***P < 0.001$). All PCR data is normalized to GAPDH. All data are mean \pm s.e.m. n are biological replicates (**B, F, G**). Statistics are one-way ANOVA with Bonferroni's post-test analysis (**B, F, G**). **A** was partially created with BioRender.com released under a Creative Commons Attribution-NonCommercial-NoDerivs 4.0 International license (<https://creativecommons.org/licenses/by-nc-nd/4.0/deed.en>).

endothelin-1 and carbachol significantly increased intracellular calcium levels in iMPCs, similar to control primary MSCs and SMCs (Fig. 2A, B). To further evaluate their contractile properties, we employed a three-dimensional collagen contractility assay. When exposed to U46619, a thromboxane A2 (TXA2) analog that acts as a potent vasoconstrictor, iMPCs contracted comparably to MSCs (Fig. 2C). These findings indicate that iMPCs can respond to vasoconstrictive stimuli, thus exhibiting a crucial functional characteristic of mural cells *in vivo*¹⁸.

We also assessed the deposition of extracellular fibronectin in iMPCs following treatment with increasing concentrations of TGF- β . Upon treatment with exogenous TGF- β , we observed a substantial increase in fibronectin production, evident at both the protein (Fig. 2D, E) and mRNA (Fig. 2F) levels. Additionally, the introduction of small molecules that inhibit TGF- β signaling (SB431542) effectively prevented fibronectin production, thereby confirming that fibronectin deposition in iMPCs is mediated by TGF- β . The capacity to deposit extracellular fibronectin represents a key functional property of mural cells¹⁹.

Central to mural cell function is their capacity to interact with ECs by producing angiogenic factors. We investigated the ability of iMPCs to modulate EC behavior through the secretion of paracrine pro-angiogenic factors and compared it to that of SMCs and MSCs by examining their respective conditioned media using an angiogenesis protein array (Fig. 2G) and quantitative Luminex assay (Fig. 2H). Notably, iMPCs secreted various pro-angiogenic factors, including VEGF-A, PLGF, HB-EGF, HGF, several members of the IGF1 family, as well as members of the serine protease inhibitor (serpin) superfamily of proteins (Serpin E1 and Serpin F1) and urokinase-type plasminogen activator (uPA), among others. The levels of these factors varied among groups, with some being significantly more abundant in iMPCs (e.g., PLGF, HGF), while others were less prominent in iMPCs compared to primary SMCs (FGF2, VEGF-A, VEGF-C). Nevertheless, the overall pro-angiogenic secretome of iMPCs was consistent with what is expected for mural cells²⁰.

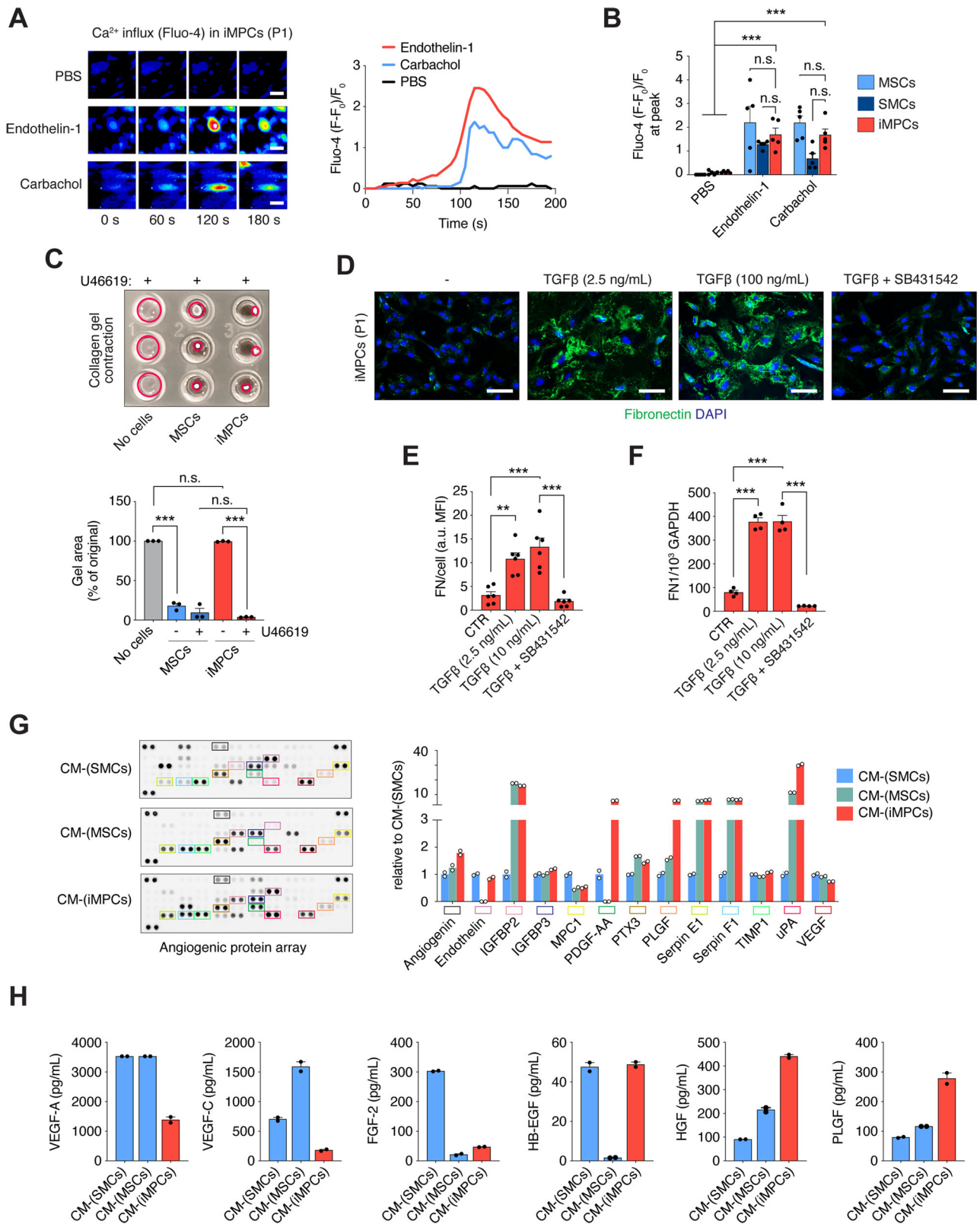
Modulation of EC function by iMPCs

To investigate whether proteins secreted by iMPCs could modulate EC activity, we exposed human umbilical cord blood-derived endothelial colony-forming cells (ECFCs, referred to herein as ECs) to medium conditioned by iMPCs (CM-iMPCs) in three different *in vitro* functional assays (Fig. 3). Firstly, using a standard proliferation assay, we observed that direct exposure to CM-iMPCs (Fig. 3A) promoted EC mitogenesis, as the number of ECs exposed to CM-iMPCs for 72 h was significantly higher than the number observed when cells were exposed to a basal control medium. Furthermore, EC proliferation was comparable to that observed upon exposure to CM-SMCs and CM-MSCs. Similarly, CM-iMPCs significantly enhanced the ability of ECs to migrate and re-endothelialize scratched monolayers (Fig. 3B), as well as to assemble into capillary-like structures in three-dimensional cultures (Fig. 3C). Overall, our data indicate that iMPCs effectively modulate EC function *in vitro* through the secretion of paracrine factors, and their capacity to influence EC activity is comparable to that of control mural SMCs and MSCs.

To evaluate a more physiologically relevant assay, we used an established *in vitro* model that cocultures iMPCs directly with ECs in a three-dimensional (3D) hydrogel. This microphysiological system—a microfluidic ‘on-a-chip’ model—facilitates the dynamic interaction of cells and the formation of a microvascular network through vasculogenesis. First, we combined GFP-labeled iMPCs and DsRed-labeled ECs within a fibrin gel and examined the ability of the iMPCs to enable vascular morphogenesis (Fig. 3D). This setup led to the formation of vascular structures lined by the DsRed+ ECs within 2 days (Fig. 3D). Furthermore, immunofluorescent staining confirmed the formation of a vascular network within the chip with a continuous endothelial lining marked by CD31 and VE-Cadherin and the presence of α -SMA+ and SM22+ iMPCs serving as perivascular cells adjacent to some of the EC-lined lumens (Fig. 3E). This ‘on-a-chip’ model confirmed the potential of iMPCs, when cocultured with ECs, to assemble complex vascular networks, hence supporting their functionality as mural cells.

To determine whether iMPCs can function as perivascular cells and support blood vessel formation *in vivo*, we implanted iMPCs together with ECs subcutaneously into immunodeficient mice (Fig. 3F–K). One week post-implantation, we removed the implants and analyzed them for the formation of human-specific vascular networks. Macroscopic examination of the explanted grafts revealed blood perfusion only in those containing ECs with mural cells (either SMCs, MSCs, or iMPCs) (Fig. 3F). Indeed, H&E staining confirmed that all implants seeded with mural cells had formed numerous perfused blood vessels containing murine erythrocytes (Fig. 3G), while grafts with ECs alone failed to form perfused vessels. Careful examination of the blood vessels showed no histological signs of hemorrhage or thrombosis (i.e., platelet aggregation and uniform fibrin deposition), indicating proper functionality. Quantification of the average microvessel densities at day 7 revealed no statistically significant differences between implants prepared with each of the different mural cell populations (Fig. 3H). The ability of iMPCs to support vascular networks *in vivo* was corroborated using another source of primary ECs. Grafts containing human umbilical vein endothelial cells (HUVECs) and iMPCs yielded mature and perfused vessels, as evidenced by human-specific CD31 staining and the presence of human perivascular cells (Supplementary Fig. 7).

The generation of EC-lined vascular structures depended on the presence of mural cells. Perfused vessels stained positively for human-specific CD31, indicating that the newly formed human vasculature had established functional anastomoses with murine host blood vessels (Fig. 3I). Perivascular involvement of α -SMA-expressing iMPCs was confirmed by human-specific vimentin staining observed in cells surrounding the human EC-lined microvessels (Fig. 3I). In designated experiments, we employed GFP-labeled iMPCs to track their *in vivo* location. Double staining of GFP and α -SMA revealed that, after 7 days *in vivo*, GFP-expressing iMPCs were primarily detected in proximity and immediately adjacent to luminal structures (Fig. 3J), indicating their structural participation in the perivascular compartment of newly formed blood vessels. Quantification of mural cell investment revealed that a substantial majority (>90%) of the human vessels exhibited perivascular coverage, with a significant proportion of these vessels being invested by the transplanted iMPCs (Fig. 3K).



In summary, our data demonstrate that iMPCs were capable of modulating EC function in vitro and in vivo to the same extent as the control mural SMCs and MSCs.

Maturation of iMPCs upon interaction with ECs

Interactions between mural progenitor cells and ECs play a pivotal role in vascular blood vessel development, maturation, and

stabilization^{21,22}. Concurrently, these interactions drive the mural progenitors into mature terminally differentiated mural cell types²³. To examine the maturation potential of our NKX3.1-induced iMPCs, we subjected them to a seven-day co-culture with ECs, resulting in co-iMPCs. We then compared iMPCs and co-iMPCs (sorted as CD31+ cells from the co-culture) using bulk RNA-seq (Fig. 4). This comparison revealed thousands of differentially expressed genes between iMPCs

Fig. 2 | Functional assessment and secretory profile of iMPCs. **A** Calcium Imaging: Intracellular calcium flux in iMPCs at Day 4 visualized using a green fluorescent indicator following stimulation with endothelin-1, carbachol, or PBS. Pseudo-coloring indicates intensity, with blue and red representing lower and higher calcium levels, respectively (Scale bars: 40 μ m). Quantitative analysis of peak calcium uptake is shown on the right. **B** Peak Calcium Response: Comparative uptake in MSCs, SMCs, and iMPCs upon endothelin-1 and carbachol stimulation, shown as delta fluorescence ($n = 5$; $***P < 0.001$). **C** Collagen Gel Contraction: Image and analysis of gel contractility by iMPCs and MSCs in response to U46619 (TXA2 analog) ($n = 3$; $***P < 0.001$). **D, E** Fibronectin Deposition: Immunofluorescence

staining of iMPCs treated with TGF β and TGF β inhibitor SB431542 (Scale bars: 100 μ m), with quantification of fibronectin intensity per cell shown in **(E)** ($n = 6$; $**P < 0.01$, $***P < 0.001$). **F** FNI Expression: RT-qPCR analysis of FNI normalized to GAPDH ($n = 4$; $***P < 0.001$). **G** Secretome Profiling: Analysis of 55 angiogenic proteins in conditioned media from iMPCs versus SMCs and MSCs, with quantification using Cellpose (Right) ($n = 1$). **H** Angiogenic Factor Quantification: Multiplex assay of angiogenic factors in conditioned media, including FGF-2, HB-EGF, HGF, PLGF, VEGF-A, and VEGF-C ($n = 2$). All data are mean \pm s.e.m. n are biological replicates (**B, C, E, F, H**). Statistics are one-way ANOVA with Bonferroni's post-test analysis (**B, C, E, F, H**).

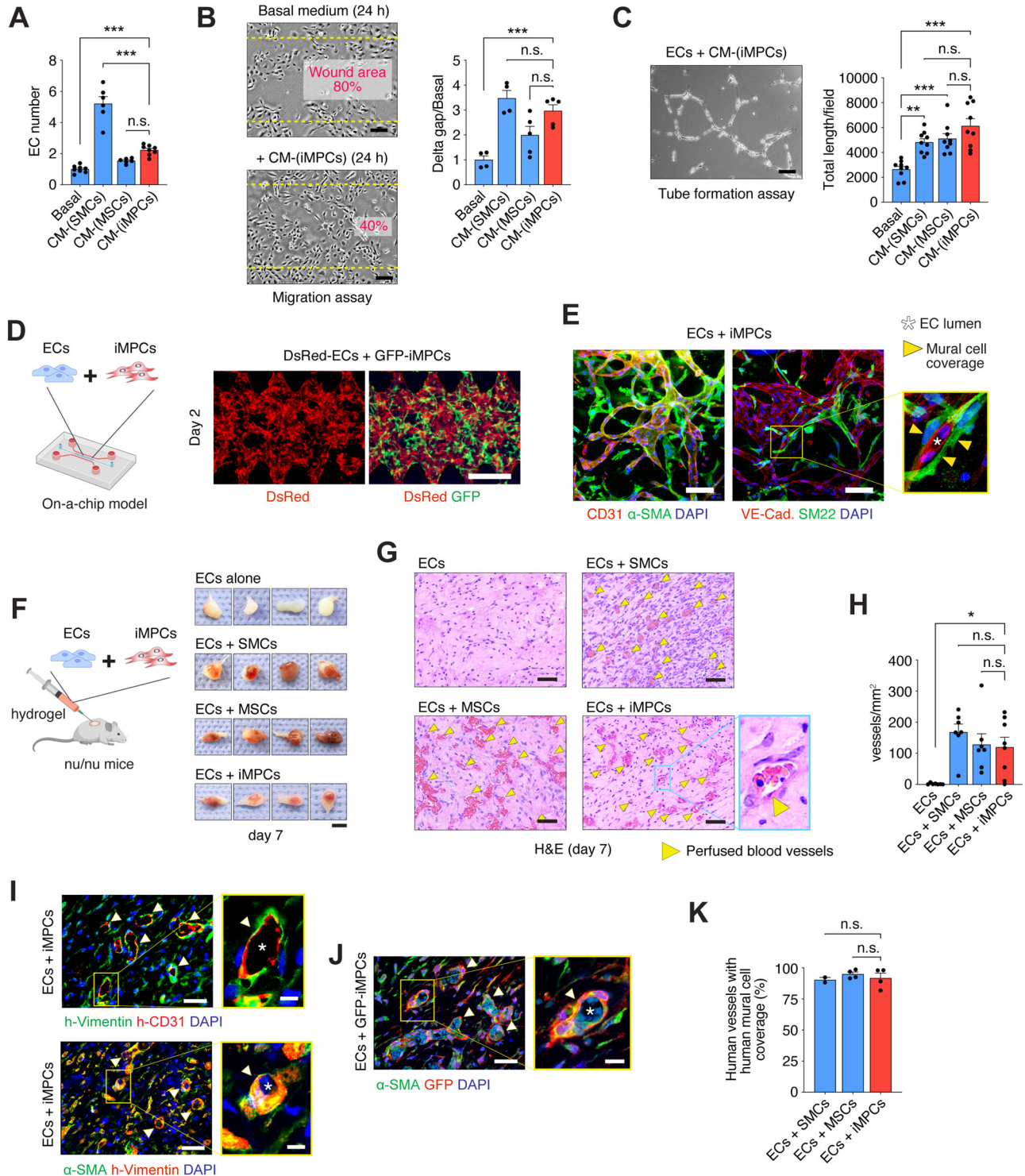


Fig. 3 | iMPCs regulate endothelial cell function. **A** Growth quantification in ECs exposed to 2-fold concentrated conditioned medium from SMCs, MSCs, and iMPCs ($n = 6, 8$; $***P < 0.001$). **B** Scratch assay comparing EC migration in conditioned medium from iMPCs and basal medium at 24 h (Left; Scale bar: 200 μm), with a quantified migration percentage of gap closure normalized to the basal medium control (Right; $n = 4$; $***P < 0.001$). **C** Tube formation assay on Matrigel using conditioned medium, with a representative image (Scale bars: 200 μm) and quantification of total tube length (Right; $n = 9$; $**P < 0.01$, $***P < 0.001$). **D** Schematic representation and fluorescent images showing the coculture of ECs and iMPCs (PI) within a microfluidic on-a-chip model. GFP-labeled iMPCs and DsRed-labeled ECs were embedded in a fibrin gel, and the formation of vascular structures was observed after 2 days. (Scale bars: 500 μm). **E** Immunofluorescent staining of the vascular network formed within the microfluidic chip. ECs are marked by CD31 and VE-Cadherin (red), and iMPCs by α -SMA and SM22 (green). Nuclei are counterstained with DAPI (blue). The inset shows a magnified view of an endothelial lumen surrounded by mural cells (yellow arrowheads). (Scale bars: 100 μm).

F Subcutaneous implantation of ECs with or without mural cells into nude mice, with explanted grafts visually assessed at day 7 (Scale bar: 4 mm). **G** H&E staining identifying perfused blood vessels in implants at day 7 (yellow arrowheads) (Scale bars: 50 μm). **H** Microvessel density analysis per mm^2 area ($n = 7$; $*P < 0.05$). **I** IHC showing human-specific ECs (h-CD31+) and human perivascular cells (h-Vimentin+) (Scale bar: 50 μm ; inset 10 μm). **J** iMPC Tracing: GFP and α -SMA staining to track GFP-labeled iMPCs within the perivascular niche in vivo. (Scale bars: 50 μm ; insets 10 μm). **K** Quantification of the percentage of human vessels with human mural cell coverage, comparing ECs implanted with SMCs, MSCs, and iMPCs ($n = 4$). All data are mean \pm s.e.m. n are biological replicates (**A–C, H, K**). Statistics are one-way ANOVA with Bonferroni's post-test analysis (**A–C, H, K**). **D, F** were partially created with BioRender.com released under a Creative Commons Attribution-NonCommercial-NoDerivs 4.0 International license (<https://creativecommons.org/licenses/by-nc-nd/4.0/deed.en>).

and co-iMPCs (Fig. 4A). Moreover, hierarchical clustering analysis showed that co-iMPCs aligned transcriptionally more closely with primary SMCs and MSCs than iMPCs (Fig. 4D). Pairwise correlation (Fig. 4B) and principal component analyses (Fig. 4C) further confirmed this hierarchical association.

We conducted gene ontology (GO) enrichment analyses to investigate these transcriptional differences in depth. We found a significant enrichment in co-iMPCs of genes related to mature mural cell functions, including ECM organization, regulation of vasculature, smooth muscle cell contraction, and connective tissue development (Fig. 4E). In addition, our qPCR analysis showed an evident upregulation of several mural cell genes in co-iMPCs relative to iMPCs. These included SMC-associated genes, such as *ACTA2*, *CNN1*, *TAGLN*, *MYOCD*, and *TPMI* (Fig. 4F), as well as pericyte-related genes like *CSPG4* and *PDE5A* (Fig. 4G). Of note, control iMPCs cultured in the same media for seven days without ECs did not exhibit the upregulation of mature mural markers observed when co-cultured with ECs (Supplementary Fig. 8). This general upregulation pattern in co-iMPCs mirrored that observed in primary MSCs after a seven-day co-culture with ECs, underscoring the widely recognized progenitor role of MSCs²⁴.

Moreover, immunofluorescence staining of co-iMPCs confirmed the separate presence of both 3G5+ pericytes (the 3G5 ganglioside antigen is expressed on the cell surface of pericytes) and α -SMA + /3G5-SMCs (Fig. 4H). This 3G5 ganglioside antibody was previously validated to accurately label pericytes in both culture and clinical samples^{25,26}. Moreover, studies have corroborated that 3G5 is not found in vascular SMCs and have utilized the 3G5 antibody for pericyte identification and isolation across various tissues, including human skin and mouse hearts^{27–29}. Thus, the 3G5 ganglioside is accepted as a reliable marker for identifying pericytes.

Lastly, it is important to note that iMPCs exhibited only minimal MYH11 expression (a mature SMC marker) before co-culture with ECs at both the mRNA and protein levels (Fig. 4F, I). This is consistent with the well-documented observation that MYH11 expression is generally subdued in SMCs when cultured in isolation. Instead, robust expression of MYH11 is typically reported in vivo, in freshly isolated cells, or in coculture systems that facilitate interactions with ECs. Indeed, upon 7-day coculture of iMPCs with ECs, we observed some cells displayed high levels of both MYH11 and α -SMA, while others exhibited high MYH11 but low α -SMA (Fig. 4I), suggesting a heterogeneous mixture of mural cell phenotypes. This protein-level evidence supports the presence of MYH11+ SMCs among the generated mural cells and reinforces the contextual dependency of MYH11 expression in SMCs.

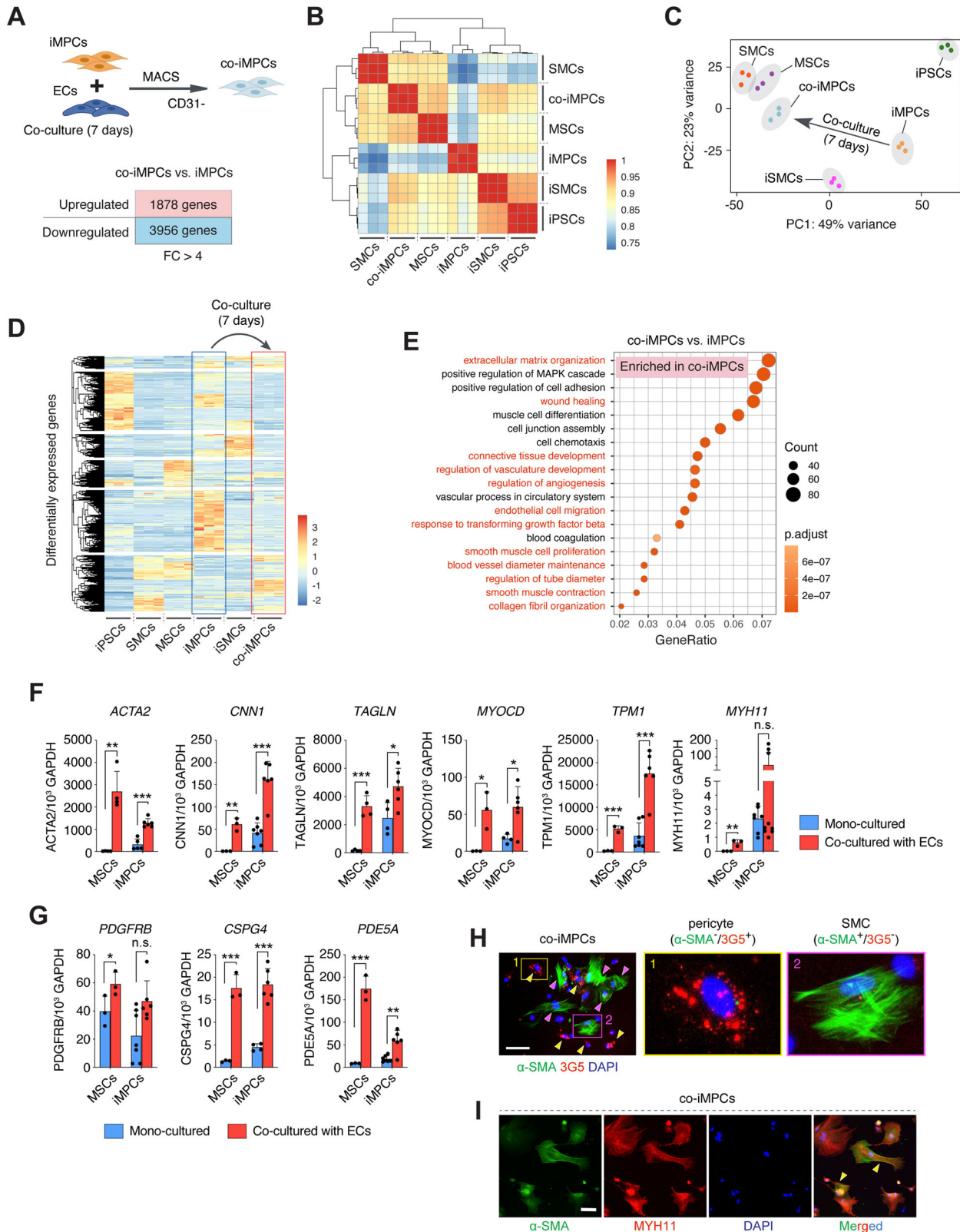
Taken collectively, these results indicate that NKX3.1-induced iMPCs are not passive EC function regulators. Instead, they display an active, dynamic response to EC interaction that leads to a significant maturation into mural cells. This ability to differentiate, characterized

by a distinct upregulation of mature mural cell-associated genes, underscores the progenitor nature of iMPCs.

Recapitulation of mural cell heterogeneity by iMPCs

Our previous analyses using immunofluorescence and qPCR demonstrated that iMPCs express markers typical of multiple mural cell types, including SMCs and pericytes (Fig. 4). To further investigate the extent to which iMPCs can recapitulate mural cell heterogeneity, we employed single-cell RNA sequencing (scRNA-seq) to examine the differentiation of iPSCs into iMPCs as well as the interaction between iMPCs and ECs (Fig. 5). Specifically, we sampled four critical stages of our differentiation protocol corresponding to day 0 (iPSCs), day 2 (MePCs after mesodermal differentiation), day 4 (iMPCs after NKX3.1 activation), and day 11, following a seven-day co-culture of iMPCs with ECs (Fig. 5A). The goal was to determine whether co-culturing with ECs enhances iMPC maturation and diversifies the mural cell population into recognizable perivascular cell types. We used the 10X Genomics platform to obtain data from 10,000 cells at each differentiation stage. The Seurat software facilitated normalization across these time points and enabled integrated cell clustering, resulting in the identification of nine discrete cell populations based on the expression of characteristic cellular markers (Fig. 5B, D, and Supplementary Figs 9–12). The annotated populations included 1) iPSCs (Cluster #1, marked by *OCT4*, *NANOG*, and *SOX2*), 2) MePCs (Cluster #2, expressing *TBX6*, *MSGN1*, *MIXL1* and *TBXT*), 3) iMPCs (Cluster #3) that exhibited high levels of *NKX3.1*, expressed *CSPG4*, *PDGFRB*, and *DES*, but had reduced expressions of genes encoding for CD73 (*NTSE*) and contractile proteins (*ACTA2*, *CNN1*, and *TAGLN*), and 4) a fibroblast-like population (Cluster #4) that was characterized by high *NKX3.1*, *PDGFRB*, *ACTA2*, and *PDGFRA* expression and lacked *NTSE* expression (Fig. 5D, and Supplementary Figs. 9–12). Of note, the expression of *PDGFRA* was prominent in cluster #4 compared to the other annotated mural cell populations, which aligns with common criteria used in the field for identifying fibroblasts³⁰. The temporal evolution of these clusters was consistent with the progression from iPSCs (day 0) to MePCs (day 2) and then to iMPCs (day 4) (Fig. 5C).

Additionally, we analyzed our scRNA-seq data for markers associated with paraxial mesoderm (*TBX6*, *MSGN1*), somites (*FOXC2*, *MEOX2*, *TCF15*), and sclerotome (*PAX9*, *SOX9*, *NKX3.2*)^{31,32} (Supplementary Fig. 10). At the mesodermal stage (MePCs at day 2, before NKX3.1 activation), *TBX6* and *MSGN1* were detectable, aligning with their expected expression in early mesodermal differentiation. However, post NKX3.1 activation at day 4 (iMPCs), these markers were not prominently expressed, suggesting a transition away from a general mesodermal identity towards a more defined lineage. Markers associated with somite and sclerotome differentiation showed negligible expression on day 2, and only *FOXC2* and *SOX9* showed some expression on day 4 in iMPCs (Supplementary Fig. 10). This pattern



indicates a minimal influence of NKX3.1 activation on inducing somite or sclerotome identities directly from MePCs.

We also analyzed interactions between iMPCs and ECs. After 7 days of co-culture with ECs, iMPCs matured into three distinct mural cell subpopulations (clusters #5, #6, and #7 at day 11; Fig. 5B, C). These mural cell clusters no longer expressed *NKX3.1*, confirming its transient activation, but uniformly expressed general perivascular markers

PDGFRB and *NTSE* (*CD73*). Of note, while iMPCs resembled nascent pericytes, mural cell clusters after co-culture with ECs resembled mature perivascular cells, including pericytes (cluster #5), contractile SMCs (c-SMCs; cluster #6), and synthetic SMCs (s-SMCs; cluster #7). These clusters, while sharing the expression of *PDGFRB*, exhibited important differences, particularly with respect to genes associated with contractile proteins and ECM production (Fig. 5E). Indeed, a direct

Fig. 4 | Maturation of iMPCs upon interaction with ECs. A Co-Culture and Transcriptomics: Diagram showing iMPCs and ECs in co-culture for bulk RNA sequencing. The lower panel indicates up-regulated and down-regulated gene counts in co-cultured iMPCs (co-iMPCs) versus mono-cultured iMPCs. **B** Transcriptomic Correlation: Pearson's correlation plot delineating transcriptional profiles among SMCs, co-iMPCs, MSCs, iMPCs, sSMCs, and iPSCs. **C** Principal Component Analysis: Transcriptional comparison of co-iMPCs with primary SMCs and MSCs relative to iMPCs and iPSCs ($n = 3$). **D** Gene Expression Heatmap: Differential gene expression patterns in co-iMPCs compared to iMPCs. **E** Gene Ontology Enrichment: Up-regulated genes in co-iMPCs associated with mature mural cell functions. **F, G** Marker Gene Expression: RT-qPCR analysis of (F) SMC and (G) pericyte markers, showing enhanced expression in co-iMPCs versus mono-cultured iMPCs ($n = 3, 4, 6, 7, 9$; $*P < 0.05$, $**P < 0.01$, $***P < 0.001$). All PCR data is

normalized to GAPDH. **H, I** Immunofluorescence Characterization of co-iMPCs: co-iMPCs were sorted as CD31⁺ cells from the co-culture. **H** Sorted cells stained for α -SMA (green) with 3G5 (pericyte marker, red) and nuclei counterstained with DAPI (blue), demonstrating the presence of both SMCs (α -SMA⁺ /3G5⁻) and pericytes (α -SMA⁺ /3G5⁺) (Scale bar: 100 μ m). **I** Sorted cells stained for α -SMA (green), MYH11 (red), and DAPI (blue). The co-localization of MYH11 and α -SMA is indicative of cells with a more mature SMC phenotype (yellow arrowheads). (Scale bar: 50 μ m). All experiments in this Figure used nascent iMPCs right after differentiation (96 h). All data are mean \pm s.e.m. n are biological replicates (F, G). Statistics are one-way ANOVA with Bonferroni's post-test analysis (F, G). A was partially created with BioRender.com released under a Creative Commons Attribution-NonCommercial-NoDerivs 4.0 International license (<https://creativecommons.org/licenses/by-nc-nd/4.0/deed.en>).

comparison of differentially expressed genes revealed a significant upregulation in genes encoding for cell contractility (e.g., *ACTA2*, *CNN1*, *TAGLN*) and ECM proteins (e.g., *FNI*, *COL1A1*, *COL1A2*) in SMCs compared to pericytes (Cluster #5) (Fig. 5E), which is consistent with their perivascular roles in vivo¹³³. Meanwhile, a direct comparison between the two clusters of SMCs revealed a clear distinction between the contractile (e.g., upregulation of *ACTA2*, *MYL9*, *TAGLN*) and the synthetic (e.g., *FNI*, *COL5A1*, *COL4A1*) phenotypes of c-SMCs and s-SMCs, respectively (Fig. 5E), consistent with the previous description of these two types of SMC manifestations^{33,34}.

Additionally, we expanded our comparative analysis to evaluate the similarity between our iMPC-derived mural cells (i.e., after co-culture with ECs) and primary mural cells. First, we conducted comparative analyses with publicly available bulk RNA datasets to provide a more precise context. We specifically compared our scRNA-seq data from cells characterized as SMCs (clusters #6 and #7 in Fig. 5) to human aortic SMCs in public datasets. Similarly, our cells identified as pericytes (cluster #5 in Fig. 5) were compared to public datasets of primary human brain pericytes. Pearson correlation analysis of these comparisons demonstrated robust correlations (correlation coefficient -0.6 , $p < 0.001$) for both sets of comparisons, indicating a substantial transcriptional alignment of our derived mural cells with public datasets (Supplementary Fig. 13A, B).

Furthermore, to establish an additional unbiased benchmark, we used the comprehensive Tabula Sapiens Consortium's vasculature dataset³⁵. This dataset encompasses a diverse array of vascular endothelial and mural cell types. By overlaying our scRNA-seq data at day 11 (i.e., mural cells generated from iMPCs after 7 days of co-culture with ECs), we observed that our cells identified as SMC-like clusters (clusters #6 and #7 in Fig. 5) exhibited substantial overlap with the reference SMCs (4832 of our SMCs matched the reference Tabula Sapiens SMCs; Supplementary Fig. 13C). Similarly, most of our cells categorized as pericytes (cluster #5 in Fig. 5) closely matched with reference pericytes (808 of our pericytes matched the reference Tabula Sapiens pericytes; Supplementary Fig. 13D). This analysis indicates that most of our SMCs align strongly with established reference SMCs. It also shows that cells from our pericyte cluster show more similarity to the reference pericytes than to SMCs or fibroblasts.

These comparative evaluations demonstrate that the gene expression profiles of our iMPC-derived SMCs and pericytes exhibit significant congruence with established primary human mural cells and a detailed single-cell reference from The Tabula Sapiens Consortium, suggesting the relevance of our differentiation model to in vivo counterparts.

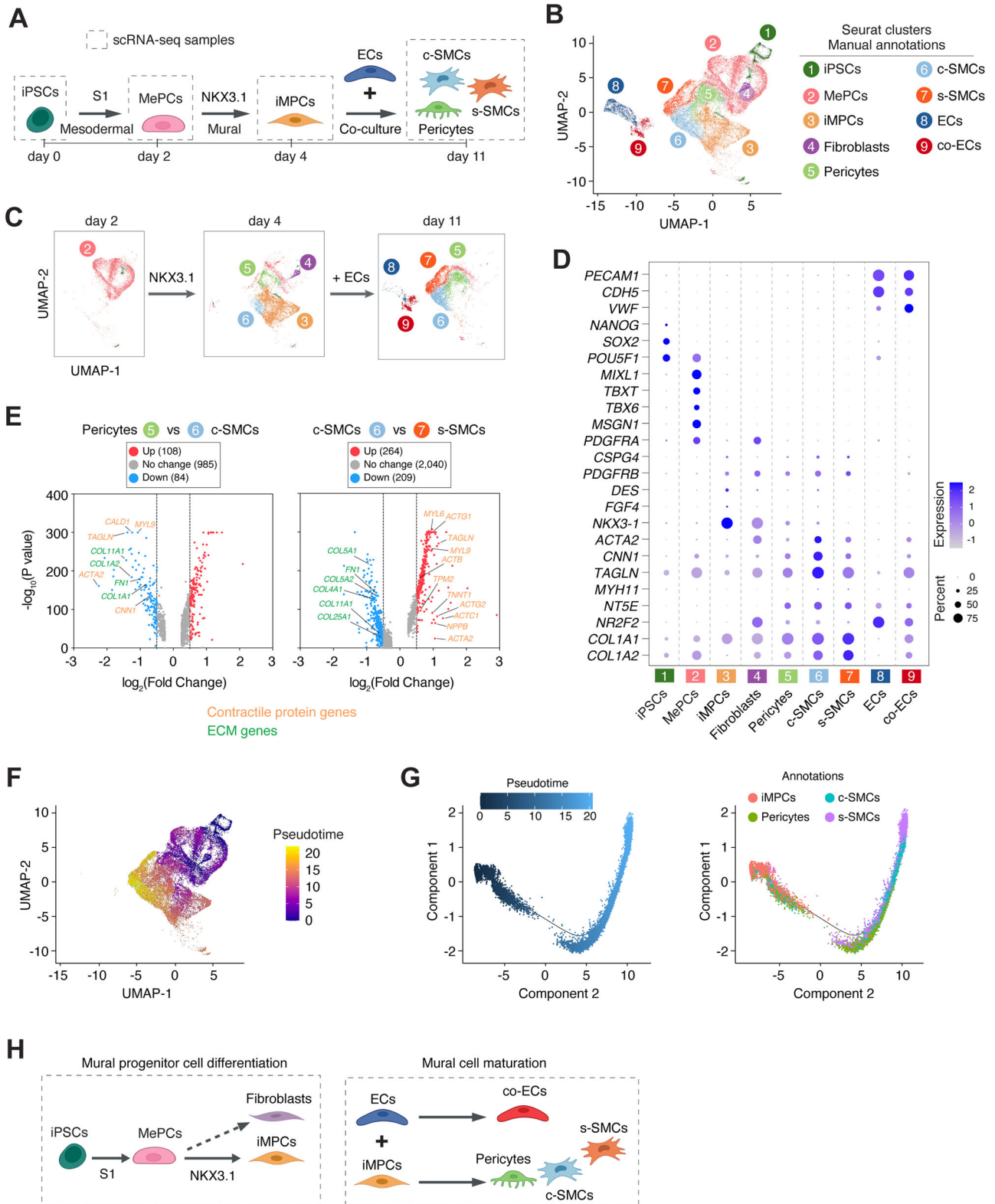
In order to gain further insights into the signals involved in mural cell differentiation and maturation, we examined the cell non-autonomous signals derived from ECs that promote mural cell maturation. Using CellChat to analyze our scRNA-seq data, we identified several key signaling pathways, notably NOTCH and TGF- β , which are known to be implicated in vascular and mural cell development^{36,37} (Supplementary Fig. 14A, B). To confirm the functional importance of

these pathways, we conducted in vitro assays where iMPCs were co-cultured with ECs in the presence of specific pathway inhibitors (Supplementary Fig. 14C). The inhibition of NOTCH signaling with DAPT significantly impaired the maturation of iMPCs in both pericyte and SMC phenotypes, confirming the role of NOTCH in mural cell maturation (Supplementary Fig. 14D). Similarly, inhibition of TGF- β signaling with SB431542 selectively disrupted SMC maturation, indicating its pivotal role in this process while preserving a pericyte-like phenotype (Supplementary Fig. 14E).

Our analysis also included examining the differential gene expression profiles between nascent and more mature pericytes (clusters #5 at days 4 and 11, respectively). We identified distinct gene signatures differentiating early-stage pericytes from their mature counterparts. GO pathway analyses of these DEGs revealed that day 11 pericytes exhibited significant enrichment in genes associated with ECM organization, cellular adhesion, and TGF- β signaling pathways, indicative of a mature mural cell phenotype (Supplementary Fig. 15). In contrast, days 4 pericytes showed enriched expression in genes linked to cell proliferation, regulation of cell differentiation, and Wnt signaling pathways, reflecting their developmental stage closer to mesodermal progenitors (see DEGs in Supplementary Data 1). Moreover, GO and KEGG analyses of differential gene expression between pericytes (cluster #5) and c-SMCs (cluster #6) confirmed significant enrichment in functions associated with ECM organization, cell-matrix adhesion, cellular contractility, and various signaling pathways related to TGF- β signaling in c-SMCs (Supplementary Fig. 15), indicative of the contractile and structural roles typically associated with SMCs.

Next, we performed an in-depth analysis of our scRNA-seq data to elucidate the gene regulatory networks (GRNs) driving the differentiation of our mural cell populations from MePCs into iMPCs, pericytes, and SMCs (Supplementary Fig. 16). Using a combination of TF motif enrichment analysis and gene expression correlation mapping, we identified distinct GRNs that govern the progression from MePCs to mature mural cells, including pericytes and SMCs (Supplementary Fig. 16A). This approach leveraged regulatory elements predicted to be active in each cell state, providing a dynamic view of the transcriptional controls that shape cell fate decisions. For instance, in early-stage MePCs, these networks included regulators such as MIXL1 and MSX1, which are pivotal during mesodermal specification (GRN9, Supplementary Fig. 16B). Later, several GRNs were highly active in iMPCs compared to mature SMCs and pericytes (GRN4 and GRN12, Supplementary Fig. 16B), suggesting that genes included in these GRNs, such as TIMP1, TGFB1, JAK, and PIEZO1, could be influenced by NKX3.1. As the cells progressed toward a more defined mural cell fate, we observed a transition in the active GRN10, with an increased representation of motifs related to TGF- β signaling (TGFB2), ECM production, and contractile function—key aspects of mature mural cell phenotypes (Supplementary Fig. 16B).

Lastly, our trajectory analyses with pseudotime plots provided further insights into the temporal evolution from iPSCs to MePCs and subsequently to iMPCs (Fig. 5F). This analysis also confirmed that iMPC



interaction with ECs promoted the development of the various mature mural cell subpopulations, starting with pericytes and progressing to c-SMCs and s-SMCs. Additional pseudotime analysis provided a more precise visualization of the developmental trajectory and maturation stages of different cell subsets derived from iMPCs (Fig. 5G). This pseudo-time trajectory analysis indicated that the pericyte cluster appears temporally closer to the iMPCs than the SMC clusters, suggesting an earlier stage in pericyte development. This is consistent

with the notion that iMPCs resemble nascent pericytes. On day 11, the pericyte cluster (#5) manifests earlier than the synthetic SMC cluster (#7) (Fig. 5G), highlighting a developmental hierarchy. Furthermore, our analyses revealed insights into the origins of s-SMCs during co-culture maturation stages. Pseudotime trajectory analysis suggests that synthetic SMCs (s-SMCs) represent a later stage of mural cell differentiation, emerging from contractile SMCs (c-SMCs) under the influence of continuous endothelial interaction, highlighting the

Fig. 5 | Delineation of mural cell heterogeneity and maturation in iPSCs via scRNA-seq. **A** Differentiation and Co-Culture Timeline: Schematic illustrating the progression from iPSCs through various stages to iMPCs and their subsequent co-culture with ECs, with an emphasis on the transition points sampled for scRNA-seq. c-SMCs and s-SMCs refer to contractile and synthetic SMCs, respectively. **B** Cellular Clustering: UMAP projection displaying identified clusters annotated into nine cell types, including iPSCs, MePCs, iMPCs, and various mural cells, based on gene expression markers. **C** Differentiation Trajectory: UMAP visualization tracking the differentiation from iPSCs to iMPCs and the emergence of mural cell clusters. **D** Marker Gene Expression: Dot plot summarizing the expression profiles of key markers across clusters, delineating cell identity. **E** Gene Expression Dynamics:

Volcano plots displaying the up- and down-regulated genes in iMPCs after EC co-culture, with emphasis on genes related to contractility and ECM components. **F** Pseudotime Analysis: UMAP overlaid with pseudotime scores, indicating the developmental progression of cells. **G** Pseudotime Analysis: Differentiation trajectory from iMPCs to pericytes and SMCs, with annotations indicating distinct cell identities. **H** Schematic Summary: Illustration summarizing the differentiation of iMPCs into specialized mural cells, highlighting the impact of EC interaction on iMPC maturation and the establishment of mural cell heterogeneity. **A, H** were partially created with BioRender.com released under a Creative Commons Attribution-NonCommercial-NoDerivs 4.0 International license (<https://creativecommons.org/licenses/by-nc-nd/4.0/deed.en>).

dynamic interplay of cell-autonomous and non-autonomous signals in mural cell diversification (Fig. 5G).

In summary, our scRNA-seq analysis substantiated the notion that iMPCs act as mural cell progenitors; after a week of co-culturing with ECs, the iMPCs diversified into distinct perivascular mural cell subpopulations, including pericytes and SMCs. This finding suggests that EC interaction is pivotal in the maturation of iMPCs, allowing for a robust recapitulation of mural cell heterogeneity (Fig. 5H).

Discussion

Our study reveals the singular capacity of the NKX3.1 to rapidly drive the differentiation of human MePCs into functionally competent iMPCs. This finding notably simplifies the complexity associated with traditional chemically induced differentiation processes, which rely on a cascade of signaling molecules to achieve cell lineage specificity. The capability to streamline the iPSC-to-mural cell differentiation process into a four-day window through the transient induction of a single TF has broad implications for both basic research and translational applications.

NKX3.1 has been implicated in SMC differentiation during development through cooperative interactions with other TFs and coactivators like SRF and Myocardin^{11,38}. However, its potential to serve as a singular fate-determining TF for iPSC-to-mural cell differentiation remained an open question. We previously participated in a comprehensive, unbiased TF screen, which included over 1500 human TFs across three human PSC lines³⁹. This screening uncovered 290 TFs capable of triggering differentiation into discernable lineages without requiring modifications in external soluble or biomechanical cues. Among the identified TFs, NKX3.1 emerged as particularly notable for its ability to direct human iPSCs toward fibroblast-like cells. In this study, the direct activation of NKX3.1 in iPSCs, thereby bypassing the MePC intermediate stage, resulted predominantly in fibroblast-like cells but not in perivascular SMCs or pericytes. However, during embryogenesis, mural cell lineages are primarily derived from mesodermal progenitors⁴⁰. Indeed, mouse models previously demonstrated a highly orchestrated expression of Nkx3.1, initiating in the paraxial mesoderm at E7.5, and gradually concentrating adjacent to the dorsal aorta's endothelium by E9.5. By E11.5-15.5, Nkx3.1 was co-expressed with smooth muscle myosin heavy chain (SM-MHC) in these regions¹⁰. Zebrafish studies corroborated this mesodermal origin, showing nkx3.1 expression in mesodermal precursors specific to the trunk pericyte lineage⁴¹.

Additionally, emerging research in zebrafish demonstrates that nkx3.1 marks precursor cells poised to differentiate into brain pericytes⁴². This study also shows the transient nature of nkx3.1 activation. This finding highlights nkx3.1's potential role in guiding cells toward a pericytic (mural) lineage, which parallels our observations regarding NKX3.1 in human iPSC-derived mural progenitor cell differentiation. While these results are from a different model system, they provide valuable context that supports our use of the term 'mural progenitor cells' for cells induced by NKX3.1 activation. Moreover, the study in zebrafish demonstrated the implication of nkx3.1 in the derivation of brain pericytes from both mesodermal and neural crest

origins⁴². Thus, although we focused on the mesodermal origin, further studies to evaluate whether our NKX3.1 induction strategy could also generate neural crest-derived mural cells are warranted.

In the present study, we show that activating NKX3.1 at the MePC stage, rather than directly in iPSCs, yields a more versatile mural progenitor cell population, which we termed iMPCs. By timing the activation of NKX3.1, we could transcend the production of merely fibroblast-like cells, generating a population of mural progenitors capable of recapitulating some of the complexity of mural cell heterogeneity. Importantly, these iMPCs exhibit functional competence as perivascular cells upon interaction with vascular ECs. Thus, our differentiation strategy offers remarkable efficiency in producing mesoderm-derived mural cells. This NKX3.1 reprogramming paradigm is an ideal platform to probe the process of mural lineage specification. The simplicity and modularity of the approach afford customizability, and it can be further tailored to activate additional genes or pathways, thereby providing a highly adaptable means for generating an array of mural cell types and studying their diverse functional roles. This flexibility is a crucial advantage for research focused on elucidating the temporal aspects of gene function and their influence on differentiation. Our NKX3.1-driven system could become a versatile tool for in vitro disease modeling and drug discovery and, ultimately, enable efficient derivation of patient-specific mural cells for precision and regenerative medicine applications.

In recent years, there has been growing interest in employing inducible TFs for cell differentiation^{9,39,43,44}. Among the most significant advantages of TF-driven differentiation is the temporal control it provides. By modulating the expression of NKX3.1 in a time-specific manner, our system allows for precise dissection of the cellular and molecular events that occur at the stage of mural cell specification. This is invaluable for gaining insights into the detailed mechanisms driving the generation of iMPCs from MePCs and offers a platform for interrogating the processes underlying cell fate decisions.

An additional advantage of TF-based approaches is the possibility of developing methods for the concurrent differentiation of multiple cell types. Simultaneously differentiating human iPSCs into cells from different lineages in a controllable manner is not trivial because each cell type requires mutually incompatible differentiating conditions. However, an orthogonal differentiation approach that relies on specific TFs could override a broad range of media cues, enabling the simultaneous generation of different cell types. Indeed, recent studies have demonstrated the potential of orthogonal programming in tissue engineering and organoid systems. For instance, Ng et al. used a model of cerebral organoids and showed the orthogonal differentiation of iPSCs into both neurons and oligodendrocytes via dox-induced transient activation of two TFs, ATOH1 and SOX9, respectively³⁹. Skylar-Scott et al. used an orthogonal differentiation approach to generate vascular ECs (via ETV2) and neurons (NGN1) from human iPSCs and produce vascularized and patterned cortical organoids within days⁴⁵, demonstrating the applicability of orthogonal programming to the vasculature. However, while the list of TFs that support efficient cell differentiation into individual cell lineages continues to grow, the identification of TFs that can be effectively leveraged for mural cell

differentiation within organoid systems remains elusive. Thus, future studies are warranted to determine whether the inducible activation of NKX3.1 could enable the incorporation of mural cells in such orthogonal programming efforts within diverse organoid models. Additionally, future studies should evaluate whether the artificial overexpression of NKX3.1 might lead to synthetic cell types not found in natural development and whether our method precisely controls the ratios of different mural cell types produced.

One focal point of our study is the validation of the functional competence of our iMPCs and their mural cell derivatives. Indeed, the functional aptitude of perivascular cells is critical for modulating EC behavior and, in turn, for their utility in vascular therapies. While ECs inherently possess self-assembly capabilities into vascular structures, robust engraftment and functional vascularization *in vivo* necessarily require perivascular cell support^{46,47}. Traditionally, these accessory cells have been sourced from primary perivascular cells, including SMCs^{48,49}, pericytes⁵⁰, fibroblasts^{51,52}, and MSCs^{53–55}. However, recent advancements have pivoted towards utilizing pluripotent cells as a personalized and inexhaustible source for perivascular cells⁴⁷.

While other protocols have successfully generated functionally competent perivascular cells from pluripotent stem cells⁵⁶, our study takes a unique TF-driven approach. Earlier chemically induced methods relied on embryoid body formation for spontaneous differentiation^{57,58}, although these were later deemed unspecific and inefficient⁵⁹. In contrast, more recent 2-D methods have proved considerably more efficient, initially inducing differentiation into an intermediate mesodermal stage via Wnt and/or Activin/Nodal pathways⁶⁰ and subsequently transforming these cells into perivascular cells through the application of specific growth factors such as PDGF-BB and TGF- β ^{8,61}. Building on these foundational methods, our NKX3.1-driven approach provides a streamlined procedure for generating functionally competent iMPCs, bypassing limitations commonly associated with media-induced methods, minimizing the risk of off-target effects and introducing a reproducible, robust framework that should facilitate standardizing the differentiation of iPSCs into mural cells.

Transcriptionally, NKX3.1-induced iMPCs align with a precursor population that resembles an immature pericyte phenotype characterized by the expression of *CSPG4*, *PDGFRB*, and *DES*, but the absence of contractile proteins such as *ACTA2*, *CNN1*, and *TAGLN*. This phenotype is distinct from those observed in the mature mural cell populations obtained upon interaction with ECs. Nevertheless, our transcriptional analyses should be carefully interpreted as they revealed a nuanced expression profile of contractile proteins in iMPCs. Specifically, while the scRNA-seq data shows minimal *ACTA2*, *CNN1*, and *TAGLN* levels in the iMPCs (cluster #3), qPCR data (Fig. 1F, G) reflect the collective expression of these proteins not only from iMPCs but also from the emerging populations of SMCs, fibroblasts, and pericytes (clusters #4, #5, #6) that are also present at day 4. These considerations are important to better understand the expression dynamics within these mixed-cell populations during differentiation. In any case, our study established that iMPCs could serve as progenitors that can differentiate into pericytes and SMCs after a week of co-culturing with ECs. We substantiated this transformation from MePCs to iMPCs to terminal mural cell populations with our single-cell RNA sequencing and trajectory analyses. Moreover, our comparative evaluations demonstrated that the gene expression profiles of our iMPC-derived SMCs and pericytes significantly align with established primary human mural cells and a detailed single-cell reference from The Tabula Sapiens Consortium, underscoring the relevance of our differentiation model to *in vivo* counterparts. However, it is important to acknowledge that transcriptional differences still exist between our iPSC-derived mural cells and primary mural cells.

Our transcriptional and functional analyses have also revealed a close alignment of iMPCs with primary MSCs, which are widely

recognized as mural progenitors, although debates about their equivalence to pericytes persist^{62,63}. Indeed, our iMPCs exhibit traits consistent with chemically-induced mesenchymal progenitors identified in previous studies as PDGFR β + CD271 + CD73- immature pericytes capable of differentiating into mature mural cells⁶¹. While further studies are needed to determine the equivalence of these various progenitor populations, our work confirms that transient activation of NKX3.1 in MePCs suffices to yield a population of iMPCs that function as mural progenitor cells exhibiting characteristics congruent with mesenchymal progenitors.

One unaddressed question in our study pertains to the fate decisions made by iMPCs when co-cultured with ECs. Although some pathways promoting mural cell differentiation are known⁶⁴, the genetic pathways that guide undifferentiated cells into mature mural cells remain incompletely elucidated. Nevertheless, our platform has demonstrated the capacity of iMPCs to generate a variety of mural cell types, such as SMCs and pericytes. Additionally, our investigation into the signals from ECs that promote mural cell maturation identified the importance of NOTCH and TGF- β signaling pathways. Using specific inhibitors, we found that blocking these pathways significantly impaired the development of mural cell characteristics, highlighting their crucial role in the maturation process. These findings underscore the potential of our platform to unravel the molecular mechanisms of mural cell differentiation.

Lastly, when interpreting the use of iMPCs as perivascular cells *in vivo*, it is important to recognize that fibroblasts also possess the capability to support vascular networks⁴⁷. Consequently, results observed in endothelial-supporting assays may not exclusively identify perivascular mural cells, as some cells might differentiate into interstitial fibroblasts. This overlap in functionality between mural cells and fibroblasts introduces complexity in defining mural cells through functional assays. Understanding this potential overlap is crucial for accurately characterizing the contributions of different cell types in vascular development and for refining the assays used to identify true mural cells.

In summary, our study introduces a robust and efficient TF-driven methodology for differentiating human iPSCs into functional iMPCs. By transiently activating NKX3.1 at an intermediary stage of differentiation, we have demonstrated remarkable differentiation efficiency as well as the functional competence of the resulting iMPCs. In addition, we have shown two distinct approaches for inducing NKX3.1: a Dox-inducible system and a genomic footprint-free modRNA method. The latter, being nonviral, nonintegrating, and inherently transient, has distinct translational advantages. From a clinical application standpoint, our method could provide a reliable pathway for generating patient-specific mural cells for regenerative medicine and disease modeling⁶⁴. Moreover, our iMPCs could offer therapeutic potential in conditions characterized by pericyte loss, such as diabetic retinopathy and stroke⁶⁵. Beyond these immediate translational applications, we anticipate our study could serve as a foundational platform offering a standardized, reproducible approach for the derivation of mural cells from human iPSCs.

Methods

Generation of Doxycycline-inducible NKX3.1 iPSC lines

The doxycycline-inducible NKX3.1 (dox-NKX3.1) cell line was generated using the piggybac (PB) transposon and transposase system. To generate Dox-NKX3.1 cell lines, we utilized the piggyBac (PB) transposon system combined with Super piggyBac transposase vectors (SBI, cat. no. PB210PA-1). The PB transposon vector harboring the NKX3.1 ORF was constructed using the Gateway cloning system, with the NKX3.1 ORF kindly provided by Dr. George Church at Harvard University. The PB dox-NKX3.1 transposon and transposase vectors were transfected via electroporation at 5:1 ratio into three independent human induced pluripotent stem cells (hiPSCs) lines that were

generated as previously reported^{66,67}. One microgram of super transposon and 5 µg of PB transposon were used to transfect the 2 million cells with use of the Neon electroporation system, following the vendor's guidelines (Invitrogen, MPK10096). Electroporation parameters were set at 1150 V for pulse voltage, and 30 ms for pulse width; two pulses were introduced. For 2 million cells, we used 3 mL of electrolytic buffer and 100-µL of resuspension buffer R in 100-µL reaction tips. The electroporated cells were seeded on a Matrigel-coated dish in mTESR plus medium (STEMCELL Technologies, 100-0276) with 5 µM Y27632 (Selleckchem, S1049). Positive cells were then selected by adding puromycin (InvivoGen, ant-pr-1) at 0.5 µg/mL. The iPSC clones were collected by manual picking. The pluripotency and reactivity to doxycycline of clone 9 were validated by qPCR, and immunostaining, and used in further experiments of this study.

Differentiation of h-iPSCs into mural progenitor cells (S1-NKX3.1)

To generate mural progenitor cells using Dox-NKX3.1-iPSCs or modified NKX3.1 RNA, we followed a 2-step differentiation over 4-day period. On the first day, we seeded Dox-NKX3.1 or BJ-273 iPSCs on a Matrigel-coated 6 well-plate (Corning, 354277) in 5 µM Y27632 in mTESR plus medium at a seeding density of 200,000 cells/well. On the following day, the medium was switched to the 6 µM of CHIR99021-containing S1 medium (Sigma-Aldrich, SML1046-25MG), which was formulated with 1X glutamax (ThermoFisher, 35050061) and 60 µg/mL ascorbic acid in Advanced DMEM/F-12 (Thermo Fisher Scientific, 12634028). The cells were then continued to culture in fresh S1 medium with fresh CHIR99021 added each day. On day 3, the cells were treated with 5 µg/mL of doxycycline (Sigma-Aldrich, D9891-10G) in S1 medium for additional two days with fresh doxycycline by changing the medium every day. For modified NKX3.1, on day 3 of differentiation, cells were dissociated by TrypLE (Thermo Fisher Scientific, 12563029), and 5 µg of RNA were transfected to 2 million cells with Neon electroporation as the same parameter set described above. Finally, the electroporated cells were plated on a Matrigel-coated 6-well plate in S1 medium. After four days of differentiation, iPSCs were maintained in SmGM-2 medium (Lonza, CC-3182) on 1% gelatin coating plate. The iPSCs are passaged twice a week until passage 2 (P2), after which the frequency is reduced to once a week. The split ratio ranges from 1:2 to 1:4, depending on the confluency.

modRNA synthesis and formulation

Chemically modRNA encoding NKX3.1 [modRNA(NKX3.1)] was generated by TriLink BioTechnologies LLC. In brief, modRNA(NKX3.1) was synthesized *in vitro* by T7 RNA polymerase-mediated transcription from a linearized DNA template, which incorporates the 5' and 3' untranslated regions (UTRs) and a poly-A tail. Specifically, NKX3.1 (ORF: ATGCTCAGGGTCCGGAGCCGCGCCCGGGGAGGCGAAAGCG GAGGGGGCCGCGCCGCGACCCCGTCCAAGCCGCTCACGTCCTTCC TCATCCAGGACATCTGCGGGACGGCGCAGCGGCAAGGGCGGCCG CACGAGCAGCCAGAGACAGCGCGACCCGGAGCCGGAGCCAGAGCCA GAGCCAGAGGGAGGACGCGCCGCGGGGGCGCAGACAGCCAGC TGAGCAGCGGGCCCGCGCCGCGCGGAGGAGCCGAGACGCTGGC AGAGCCGAGCCAGAAAGGCACTTGGGGTCTTATCTGTTGGACTCTG AAAACACTTCAGGCGCCCTTCCAAGGCTTCCCCAAACCCCTAAGCAG CCGCAGAAGCGCTCCCGAGCTGCCTTCTCCACACTCAGGTGATCGA GTTGAGAGGAAGTTCAGCCATCAGAAGTACCTGTCGGCCCCCTGAAC GGGCCACCTGGCCAAGAACCTCAAGCTCACGGAGACCCAAGTGAAG ATATGGTCCAGAACAGACGCTATAAGACTAAGCGAAAGCAGCTCTC CTCGGAGCTGGGAGACTTGGAGAAGCACTCCTCTTTGCCGGCCCTGA AAGAGGAGGCCTTCTCCCGGCCCTCCCTGGTCTCCGTGTATAACAGC TATCCTTACTACCCATACCTGCTACTGCGTGGCAGCTGGAGCCAGC TTTTGGTAA; 705 bp) was cloned into the mRNA expression vector pmRNA, which contains a T7 RNA polymerase promoter, an unstructured synthetic 5'UTR, a multiple cloning site, and a 3'UTR that was

derived from the mouse (γ-globin 3' gene). *In vitro* transcriptional reaction (1-ml scale) was performed to generate unmodified mRNA transcripts with wild-type bases and a poly-A tail. Cotranscriptional capping with CleanCap Cap1 AGTrimer yields a naturally occurring Cap1 structure. Deoxyribonucleasetreatment was used to remove DNA template. 5'-Triphosphate was removed by phosphatase treatment to reduce innate immune response. After elution through a silica membrane, the purified RNA was dissolved in ribonuclease-free sodium citrate buffer (1 mM, pH 6.4).

Isolation and maintenance of human MSCs, ECs, and SMCs

Human mesenchymal stem cells (MSCs) were isolated from discarded and de-identified bone marrow samples obtained during a clinically-indicated procedure at Boston Children's Hospital in accordance with an Institutional Review Board-approved protocol, as previously described in Lin et al.⁶⁸ and maintained in MSCGM (Lonza, PT-3001) on 1% gelatin-coated plate³. Human pulmonary artery smooth muscle cells (pSMCs; Lonza, CC-2581) and human saphenous vein smooth muscle cells (kindly donated by Dr. Joyce Bischoff, Boston Children's Hospital) served as primary SMC controls. The SMCs were cultured in SmGM-2 medium (Lonza, CC-3182) on 1% gelatin-coated plate (Sigma-Aldrich, G2500-500G). Endothelial colony-forming cells (ECFCs; herein referred to as ECs) were isolated from human umbilical cord blood obtained from the Brigham and Women's Hospital in accordance with an institutional review board-approved protocol, as described⁶⁸ and cultured in ECGM2 (Lonza, CC-3162) supplemented with 20% FBS (Genesee, 25-514) without hydrocortisone. All primary cells were used up to passage 10.

Flow cytometry analysis

Cells were dissociated into single-cell suspensions using TrypLE (Thermo Fisher Scientific, 12563029) and subsequently washed with FACS buffer formulated in PBS supplemented with 1% bovine serum albumin and 0.2 mM EDTA. For specific experiments, flow cytometry analysis was conducted after fixing the cells with 4% paraformaldehyde (PFA, Electron Microscope Sciences, 15714-S). The staining procedure involved incubating the cells with the respective antibodies for 15 min on ice at a 1:100 dilution in FACS buffer. Following incubation, the cells were washed three times with PBS buffer to remove any unbound antibodies. Flow cytometry analysis was performed using a BD Accuri C6 Plus flow cytometer (BD Biosciences), and the acquired data were analyzed using FlowJo software version 9 (Tree Star Inc., Ashland, OR). Detailed information regarding the antibodies used in the staining procedure can be found in Supplementary Table 2.

Immunofluorescence staining

Cells were seeded in tissue culture-treated polymer coverslip eight-well chamber slides (ibidi USA, Fisher Scientific, 50-305-795) or 8-well chamber slides (ibidi USA, Fisher Scientific, NC1535706) at a seeding density of 2×10^4 cells/cm². On the following day, cells were fixed with 4% paraformaldehyde (PFA) and permeabilized with 100% cold methanol at -20°C or 0.2% Triton in PBS for 15 min. After blocking with 10% of BSA for 30 mins at RT, primary antibodies were added and incubated for 1h at room temperature or overnight at 4°C. After washing three times with PBS, the cells were incubated with secondary antibodies and DAPI at room temperature for 30 min. The slides containing the stained cells were mounted using DAKO fluorescence mounting medium (Agilent, S302380-2) or directly imaged without mounting. Images were obtained using an Axio Observer Z1 inverted microscope (Carl Zeiss) and AxioVision Rel. 4.8 software. For phase contrast images, we used an AxioCam MRc5 camera with either a 5X or 10X objective lens. Validation of pluripotency was carried out using OCT4, NANOG, and SOX2. Detailed information regarding the antibodies used in the staining procedure can be found in Supplementary Table 2.

Intracellular Ca²⁺ flux detection assay

Intracellular calcium flux was measured and visualized by Fluo-4 Calcium imaging kit (Life Technologies, F10489) and we followed the manual that the vendor provided. Either pVSMC or Day4 iMPC were seeded in an 8-well chamber slide with SMGM-2 medium at 2000 cells per well density. On the following day, the cells were washed with live cell imaging solution (LCIS) buffer (ThermoFisher, A14291DJ). Fluo-4 AM loading solution was prepared by adding 20 mM glucose in live cell imaging solution (LCIS) buffer, which contained probenecid, power load and fluo-4. The 200 μ L loading solution was then added to cells and incubated for 30 min at 37 C followed by 15 min incubation at room temperature. After washing the cells, we replaced the loading solution with 20 mM glucose-LCIS buffer with 10 mM carbachol (Millipore Sigma, PHR1511), 0.1 μ M endothelin1 (Millipore Sigma, E7764-10UG) or PBS and then imaged immediately. The fluorescence images were obtained using an Axio Observer Z1 inverted microscope (Zeiss) for 5 min with 5-s intervals and the relative fluorescence level of individual cells was analyzed by ImageJ with mean intensity and normalized by $(F-F_0)/F_0$.

Collagen gel contraction assay

Prior to the experiment, cells were serum starved in basal smooth muscle cell medium (SMCM, ScienceCell, 1101) which contained 0.1% FBS in the incubator overnight. The following day, 3 mL of ice-cold collagen solution was prepared by mixing 1.8 mL of 1x DMEM with 0.3 ml FBS and 0.75 ml of Bovine Collagen-1 in a 50 ml falcon tube. The solution was kept on ice to prevent solidification when adjusting the pH to 7.4 using 0.1 N NaOH. A cell suspension was prepared at 10^6 cells/ml collagen solution and 10 μ L of cell-collagen suspension was plated in triplicate in angiogenesis μ -slide (ibidi, 81506). After plating the collagen-cell suspension, the plate was incubated at 37 °C for 30 min. Once solidified, 40 μ L of SMGM2 media was added on top of the gels with a 10 μ M U46619 vasoconstrictor. Images were captured after 72 h of incubation, with Axio Observer Z1 inverted microscope (Zeiss) at 4X objective and ZEN 3.6 (blue edition) software. The surface area of the collagen gels was quantified using ImageJ. The percentage of contraction was then calculated by comparing the final area to the initial area on day 0, using the following formula: Percentage of original gel area = (Final Area / Initial Area) \times 100.

Fibronectin deposit assay

A total of 1×10^4 induced mural progenitor cells (iMPCs) were seeded onto eight-well chamber slides (ibidi USA, Fisher Scientific, 50-305-795) or 24-well plates in Smooth Muscle Growth Medium-2 (SMGM-2). The next day, the SMGM-2 medium was replaced with fresh SMGM-2 containing either 0, 2.5, 10 or 100 ng/mL of transforming growth factor-beta (TGF β) (Prospec, CYT-716), along with or without TGF β inhibitor, SB431542 (Santa Cruz Biotech, sc-204265). The cells were then treated for 72 h. To assess fibronectin expression, the cells were fixed with 4% PFA and stained with a fibronectin antibody (Abcam, Ab2413) in a blocking solution (1.5% BSA solution) without permeabilization followed by blocking for 30 min. Subsequently, after three times of washing, a goat anti-rabbit-488 secondary antibody was applied to facilitate detection with DAPI. Images were obtained using an Axio Observer Z1 inverted microscope (Zeiss) and ZEN 3.6 (blue edition) software and quantified the fibronectin deposit by measuring the green fluorescence intensity and dividing the number of cells which is measured by DAPI. The quantification was performed by Image J.

Mural-endothelia cell co-culture assay

To perform the co-culture assay of endothelial cells, at day 4 of differentiation, induced mural progenitor cells (iMPCs), human mesenchymal stem cells (MSCs), and endothelial colony-forming cells (ECFCs) were harvested using 300 μ L of TrypLE. A total of 5×10^4 iMPCs or MSCs and the same number of ECFCs were pre-mixed and

seeded onto a 6-well plate coated with 1% gelatin. The co-culture was carried out for a duration of 7 days in Endothelial Growth Medium-2 (EGM-2, Lonza, CC-3162). Following the 7-day co-culture period, CD31-positive cells were selectively removed using magnetic bead-based sorting (Invitrogen, 11155D). The CD31-positive endothelial cells (ECs) were separated and discarded using a magnetic separator, while the negative fractions were isolated for further analysis.

Transwell co-culture assay

The transwell co-culture experiment was conducted using a 48-well permeable transwell plate with a 3 μ m pore size (Corning, CLS3415). One day before co-culture, 1×10^3 endothelial colony-forming cells (ECFCs) were seeded in the bottom well of the transwell using K-medium. On the following day, 1×10^4 iMPCs at day 4 of differentiation were seeded on the top insert in basal Endothelial Basal Medium-2 (Lonza, EBM-2) supplemented with 5% Fetal Bovine Serum (FBS). After three days of co-culture, the ECFCs in the bottom well were fixed and stained with DAPI. Subsequently, 4 images per well were captured using an Axio Observer Z1 inverted microscope (Carl Zeiss) and AxioVision Rel. 4.8 software and the images were analyzed using ImageJ software. The analysis included the functions: Threshold at 50, Fill Holes, Watershed, and Analyze Particles size bigger than 10 pixels to quantify the stained cells.

Endothelial cell growth assay in conditioned media

At day 4 of differentiation, induced mural progenitor cells (iMPCs) were subjected to treatment with 2 mL of basal medium of Endothelial Basal Medium-2 (Lonza, 190860) supplemented with 5% FBS (Genesee, 25-514) for 24 h on a 6 well-tissue culture plate. Subsequently, 12 mL of the cultured medium was collected and filtered through a 0.22 μ m filter (VWR, 76479-016). The filtered medium was then concentrated using a 3 kDa cut-off centrifugal concentrator (Millipore, UFC900324) at 10,000 rpm for 45 min. To re-constitute the 2-fold concentrated samples, up to 6 mL of fresh EBM-2 medium was added. For the endothelial cell (EC) growth test, 96-well plates were utilized, with 1000 cells seeded per well in K-medium, formulated using Endothelial Cell Growth Medium-2 (ECGM2, Lonza, CC-3162) supplemented with 20% FBS (Genesee, 25-514) without hydrocortisone. The following day, the medium was switched to either Basal medium or the 2X conditioned medium obtained as described above for further experimentation.

Tube formation assay

Human ECFCs on Matrigel were used to perform tube formation assay. Matrigel (Corning, 354277) was thawed overnight at 4 C and 200 μ L was distributed on each well of the 24-well plate. After incubating 30 min in 37 C, ECFCs were dissociated with TrypLE (ThermoFisher, 12563029) and resuspended at 2×10^5 per mL and then distributed 50 μ L of cell suspension on top of solidified matrigel. Either basal medium with 0.5% FBS (control) or conditioned medium was used to culture. After 24 h of incubation, the images were obtained at phase contrast 5X and analyzed using Angiogenesis Analyzer plugin in ImageJ software.

Wound healing assay

5×10^4 ECFCs were seeded each well in a 24-well plate, and cultured until 100 percent confluence. Using 1000 P tips, we scratched one line in the center of the well and changed the medium to either basal medium of EBM-2 with 5% FBS or conditioned medium collected as described in EC growth assay. After 24 h of incubation, the scratched area was imaged by phase contrast 5X and analyzed the area using ImageJ.

Angiogenic array

The Proteome Profiler kit (R&D systems, ARY007) was used to analyze the expression profiles of 55 angiogenesis-related proteins. Two-fold

concentrated conditioned medium was prepared as described above and followed the instructions in the manufacturer's manual. In brief, 2 mL of blocking buffer (array buffer 7) was added to the membrane and incubated for one hour on a rocking platform shaker. During blocking, 1 mL of each sample was mixed with 0.5 mL of dilution buffer (array buffer 4), and 15 μ L detection antibody cocktail and then incubated for one hour. After the blocking buffer was removed, the sample-antibody mixture was distributed and incubated overnight at 4 °C on a rocking shaker. The membranes were washed three times with 20 mL for 10 min. Prior to streptavidin-HRP addition, a 4-well multi-dish was cleaned with distilled water and dried thoroughly. 2 mL of diluted streptavidin-HRP in array buffer 5 was added to the membrane in a 4-well dish and incubated for 30 mins on a rocking shaker. Followed by 3 times wash, 1 mL of Chemi-reagent evenly distributed onto the membrane. Lastly, we covered the membrane with the top sheet of the plastic protector and smoothed out the air bubbles, and incubated for 1 min before imaging. For image analysis, array spots were segmented using Cellpose. Expression levels were determined by calculating the product of spot size and intensity. Normalization of values for each experiment was performed by dividing them with the negative control value. Original scanned protein array immunoblots are displayed in Supplementary Fig. 17.

Angiogenic factors multiplex analysis

The protein concentration of 17 angiogenic factors was analyzed by the standard curve of the Human Angiogenesis 17-Plex Discovery Assay. The human angiogenesis 17-plex discovery assay was performed by Eve Technologies, Canada. Luminex xMAP technology was used for multiplexed quantification. The multiplexing analysis was performed using the Luminex™ 200 system (Luminex, Austin, TX, USA) by Eve Technologies Corp. (Calgary, Alberta). Seventeen markers were simultaneously measured in the samples using Eve Technologies' Human Angiogenesis & Growth Factor 17-Plex Discovery Assay® (MilliporeSigma, Burlington, Massachusetts, USA) according to the manufacturer's protocol. The 17-plex consisted of Angiopoietin-2, BMP-9, EGF, Endoglin, Endothelin-1, FGF-1, FGF-2, Follistatin, G-CSF, HB-EGF, HGF, IL-8, Leptin, PLGF, VEGF-A, VEGF-C, VEGF-D. Assay sensitivities of these markers range from 0.2–42.8 pg/mL for the 17-plex. Individual analyte sensitivity values are available in the MilliporeSigma MILLIPLX® MAP protocol.

Quantitative reverse transcription PCR

RNA was isolated with either an RNeasy kit (Qiagen, 74106) or SYBR™ Green Cells-to-CT™ Kit (ThermoFisher Scientific, 4402954). The cDNA was prepared using either reverse transcriptase III (Thermo Fisher Scientific, 4368814) or SYBR™ Green Cells-to-CT™ Kit according to the manufacturer's instructions. Quantitative PCR was performed using SYBR Green Master Mix (Thermo Fisher Scientific, A25776), and detection was achieved using the QuantStudio™ 3 Real-Time PCR System, 96-well (Thermo Fisher Scientific, A28567). The expression of target genes was normalized to glyceraldehyde-3-phosphate dehydrogenase (*GAPDH*). Real-time PCR primer sequences are listed in Supplementary Table 1. Statistical analyses Unless otherwise stated, data were expressed as means \pm SEM of the mean. For comparisons between two groups, means were compared using unpaired two-tailed Student's *t*-tests. Comparisons between multiple groups were performed by analysis of variance (ANOVA) followed by Bonferroni's post-test analysis. All statistical analyses were performed using GraphPad Prism v.9 software (GraphPad Software Inc.).

In vitro vascular network-forming 'on-a-chip' assay

We utilized the idenTx 3 Chip and Holder from AIM Biotech Pte. Ltd., following a slightly modified version of the manufacturer's guidelines. ECFCs and iPSCs were combined at a 3:1 ratio, resulting in 1.2×10^5 cells in 10 μ L, and embedded in a hydrogel solution. This hydrogel consisted of 6 mg/mL fibrinogen (Sigma, F8630) in 1x PBS at 37 °C and

50 U/mL thrombin (Sigma, T4648) in 1x PBS. The mixture was seeded into the chip's cell/gel channel. The culture medium was EGM-2, supplemented with 5% FBS and 50 ng/mL VEGF. For cell preparation, cells were suspended in a medium-diluted thrombin solution (4 U/mL), mixed with the fibrinogen solution to achieve final concentrations of 2 U/mL thrombin and 3 mg/mL fibrinogen, and applied to the chip's gel channel, allowing it to polymerize at 37 °C for 30 min. After polymerization, 15 μ L of culture medium was added to both media channels. To create a flow gradient, the medium volume was adjusted to 70 μ L on one side and 50 μ L on the other, with daily medium changes to maintain cell viability. The chip was kept at 37 °C in a 5% CO₂ environment.

Animal experiments

All animal experiments were performed at Boston Children's Hospital in accordance with the institutional guideline approved by Institutional Animal Care and Use Committee (IACUC) protocol 20-12-4327 R. Mice were housed under a 12-h dark/light cycle with ambient temperature maintained at 68–74 degrees F and relative humidity at 30–70%. For the in-vivo vascular network forming assay, we purchased the 6-week-old Athymic nude mice (Foxn1/nu mice) from Envigo and reared them according to the following immune-deficient mice guidelines.

In-vivo vascular network-forming assay

The in-vivo vascular network forming assay was carried out by co-transplanting human endothelial colony-forming cells (ECFCs) or Human umbilical vein endothelial cells (HUVEC, ATCC, CRL-1730), and mural cells in collagen mixed with fibrinogen gel, as previously described⁶⁹. In brief, the collagen/fibrinogen gel solution was prepared by combining 1.5 mg/mL collagen (Trevigen, 3442-050-01), 30 μ g/mL fibrinogen (Sigma-Aldrich, F8630-1G), 1 mg/mL human fibronectin (Millipore-Sigma, F0895-2MG) plus 25 mM HEPES and 10% FBS on ice. The two cell types, ECFCs or HUVECs (0.8×10^6) and one of the mural cell types (either iPSCs at day 4, pSMCs, or MSC; 1.2×10^6), were pre-mixed in 200 μ L of pH-neutral gel solution, and loaded into a 30 G syringe by using a 1 mL pipette. Mice were anesthetized with isoflurane, subcutaneously injected with 50 μ L of 50 μ g/mL thrombin (Sigma-Aldrich, T4648), then with 200 μ L of cell-loaded gel into the same site. Cell-gel implants were harvested after 1 week to analyze vascular formation.

Histology and immunofluorescence staining

Explanted grafts were fixed overnight in 10% buffered formalin and were washed in 70% ethanol. Fixed ex-grafts were embedded in paraffin and sectioned at 7 μ m. H&E-stained sections were used to assess micro-vessel density. The number of vessels per area (vessels/mm²) of graft was counted as the average number of erythrocyte-filled vessels (vessels/mm²) in H&E-stained sections. For immunostaining, sections were deparaffinized via xylene for 10 min and sequential immersion in ethanol and underwent antigen retrieval in citric buffer (10 mM sodium citrate, 0.05% Tween 20, pH 6.0) for 30 min at 95 °C. Sections were then blocked for 30 min in 5% BSA, and incubated with primary and secondary antibodies each for 1 h at RT. Human-specific anti-CD31 antibodies were used to stain human blood vessels and perivascular mural cells were immunostained with anti- α SMA antibodies. Anti-GFP or human-specific Vimentin antibodies were used to trace iPSC. The specific primary and secondary antibodies are detailed in Key Resources Table.

Bulk RNA sequencing

RNA extraction, library preparation, and sequencing were conducted at Azenta Life Sciences (South Plainfield, NJ, USA) as follows: Total RNA was extracted from fresh frozen cell pellet samples using Qiasymphony RNA kit following manufacturer's instructions (Qiagen, Hilden, Germany).

Library preparation with PolyA selection and Illumina sequencing.

RNA samples were quantified using Qubit 2.0 Fluorometer (Life Technologies, Carlsbad, CA, USA) and RNA integrity was checked using Agilent TapeStation 4200 (Agilent Technologies, Palo Alto, CA, USA). RNA sequencing libraries were prepared using the NEBNext Ultra II RNA Library Prep Kit for Illumina using the manufacturer's instructions (NEB, Ipswich, MA, USA). Briefly, mRNAs were initially enriched with Oligod(T) beads. Enriched mRNAs were fragmented for 15 min at 94 °C. First-strand and second-strand cDNA were subsequently synthesized. cDNA fragments were end-repaired and adenylated at 3' ends, and universal adapters were ligated to cDNA fragments, followed by index addition and library enrichment by PCR with limited cycles. The sequencing library was validated on the Agilent TapeStation (Agilent Technologies, Palo Alto, CA, USA), and quantified by using Qubit 2.0 Fluorometer (Invitrogen, Carlsbad, CA) as well as by quantitative PCR (KAPA Biosystems, Wilmington, MA, USA). The sequencing libraries were clustered on two flow cells. After clustering, the flowcell was loaded on the Illumina instrument 4000 according to the manufacturer's instructions. The samples were sequenced using a 2x150bp Paired-End (PE) configuration. Image analysis and base calling were conducted by the Control software. Raw sequence data (.bcl files) generated by the sequencer were converted into fastq files and demultiplexed using Illumina's bcl2fastq 2.17 software. One mismatch was allowed for index sequence identification.

Analysis of RNA sequencing data. After investigating the quality of the raw data, sequence reads were trimmed to remove possible adapter sequences and nucleotides with poor quality using Trimmomatic v.0.36. The trimmed reads were mapped to the *Homo sapiens* reference genome available on ENSEMBL using the STAR aligner v.2.5.2b. The STAR aligner is a splice-aligner that detects splice junctions and incorporates them to help align the entire read sequences. BAM files were generated as a result of this step. Unique gene hit counts were calculated by using feature Counts from the Subread package v.1.5.2. Only unique reads that fall within exon regions were counted. After extraction of gene hit counts, the gene hit counts table was used for downstream differential expression analysis. Using DESeq2, a comparison of gene expression between the groups of samples was performed. The Wald test was used to generate p-values and Log₂ fold changes. Genes with adjusted $p < 0.05$ and absolute log₂ fold changes > 1 were called as differentially expressed genes for each comparison. A gene ontology analysis was performed on the statistically significant set of genes by implementing the software GeneSCF. The goa_human or mouse GO list was used to cluster the set of genes based on their biological process and determine their statistical significance. A PCA analysis was performed using the "plotPCA" function within the DESeq2 R package. The plot shows the samples in a 2D plane spanned by their first two principal components. The top 500 genes, selected by highest row variance, were used to generate the plot.

Single-cell RNA sequencing

Cell and library preparation. Cells were treated with 300 µL of TrypLE for 3 minutes at 37 °C, followed by pipetting several times using a p1000 pipette. Subsequently, the dissociated cells were filtered through a FACS filter cell strainer. Single-cell RNA samples were prepared using the Chromium Next 10X genomics technique (10xgenomics, PN-1000128, PN-1000127) according to the manufacturer's protocol. Quantification of DNA samples was conducted using a Qubit 2.0 Fluorometer, and quality control assessment was performed at the Harvard core facility using Agilent TapeStation D5000. RNA sequencing libraries were subsequently prepared using the dual index kit (10xgenomics, PN-1000213) according to the manufacturer's instructions. Validation of sequencing libraries was carried out using Agilent TapeStation D1000 at the Harvard core facility.

Illumina sequencing. Illumina Sequencing was performed by MedGenome (CA, USA). Libraries were sequenced via Illumina Novaseq 6000 sequencer (Illumina, San Diego, CA). 150 PE reads were generated for a total of ~503 GB of data. Illumina raw BCL sequencing files were processed through the Cell Ranger software (10x Genomics) for generating FASTQ files and count matrixes (<https://support.10xgenomics.com/single-cell-gene-expression/software/overview/welcome>). Feature-barcode matrices were obtained from "cellranger count" for all the samples.

Dataset quality control. The single-cell sequencing datasets were processed using 10x Genomics Cell Ranger (version 7.1.0) tool sets⁷⁰. For each sample, the "cellranger count" pipeline was employed to quantify gene expression from the FASTQ files, including reads alignment, filtering, barcode scanning, and UMI counting. During this step, the GRCh38 human genome (version refdata-gex-GRCh38-2020-A) served as a reference⁷¹. Subsequently, the filtered feature barcode matrix files were imported into the Seurat package (version 4.1.0) for quality control, analysis, and exploration⁷². To eliminate doublets, the DoubletFinder package (version 2.0.3) was applied⁷³. Only cells expressing more than 200 and fewer than 9000 unique genes, with mitochondrial percentages below 20%, were retained for further analysis.

Cell clustering. Datasets normalization, scaling, dimension reduction, cell clustering, and differentially expressed genes (DEGs) identification were performed using the Seurat package (version 4.1.0). In brief, the global-scaling normalization method "LogNormalize" was applied to normalize the feature expression measurements for each cell, and then "ScaleData" function was used for linear transformation. The top 2000 most variable genes were identified using the "FindVariableFeatures" function to perform principal component analysis (PCA). The "FindNeighbors" function was used for construct a K-nearest neighbor (KNN) graph based on the first 15 principal components (PCs), and the "FindClusters" function was performed to cluster cells into different populations by the graph. DEGs for each population were identified using the "FindAllMarkers" function with default parameters.

Trajectory inference. To delineate the cell differential trajectory, Monocle3 (version 1.3.4) was employed for single-cell trajectory analysis⁷⁴. Throughout the analysis, the PCA dimension reduction algorithm and Log normalization method were used for preprocessing steps. The "reduce_dimension" function was then applied for dimensionality reduction using the UMAP algorithm. To cluster cells, the "cluster_cells" function was employed using the Leiden clustering method. Following preprocessing, dimension reduction, and cell clustering, the trajectory was built by the "learn_graph" function. The resulting trajectory structure was visualized by the "plot_cells" function.

Comparative transcriptomic analysis of iMPC-derived mural cells with publicly available mural cell data. We employed the "Scanorama" algorithm⁷⁵ to compare iMPC-derived pericytes/SMCs with publicly available mural cell data. The reference dataset used was "TS_Vasculature" from The Tabula Sapiens Consortium³⁵. For each pericyte/SMC in our scRNA-seq dataset, we identified the most similar cell type in the reference dataset and counted these occurrences. Using edgeR (version 4.0.16) for pseudo-bulk differential expression analysis, we calculated the Spearman coefficient to assess similarity between iMPC-derived and primary pericytes/SMCs. The results were visualized with Pheatmap (version 1.0.12), using ECFCs as a negative control⁷⁶.

Cell-cell interaction analysis. We used the R packages CellChat (version 1.6.1) and Monocle (version 2.22.0) to profile cell-cell communication and cell trajectory, respectively⁷⁷.

Gene Regulator Network analysis. The R package hdWGCNA was utilized to construct specific co-expression networks across cellular hierarchies⁷⁸.

Statistics and reproducibility

All experiments were independently repeated at least three times with similar results. Specifically, all micrographs presented in the figures are representative of experiments conducted on three or more independent occasions. Except where specifically mentioned, data were presented as means \pm standard error of the mean (s.e.m.). When comparing two groups, mean values were compared using unpaired two-tailed Student's *t*-tests. Multiple group comparisons were conducted through analysis of variance (one-way ANOVA) followed by Bonferroni correction. No exclusion criteria were applied to any of the analyses. All statistical calculations were performed using GraphPad Prism v.9 software (GraphPad Software Inc.). Statistical significance was set at $P < 0.05$.

Reporting summary

Further information on research design is available in the Nature Portfolio Reporting Summary linked to this article.

Data availability

The RNA sequencing and single-cell RNA sequencing datasets generated and/or analyzed during the current study have been deposited in the Gene Expression Omnibus (GEO) under accession number [GSE251718](https://www.ncbi.nlm.nih.gov/geo/query/acc.cgi?acc=GSE251718). Source data are provided with this paper.

References

- Armulik, A., Genové, G. & Betsholtz, C. Pericytes: developmental, physiological, and pathological perspectives, problems, and promises. *Dev. Cell* **21**, 193–215 (2011).
- Potente, M., Gerhardt, H. & Carmeliet, P. Basic and therapeutic aspects of angiogenesis. *Cell* **146**, 873–887 (2011).
- Bergers, G. & Song, S. The role of pericytes in blood-vessel formation and maintenance. *Neuro-Oncol.* **7**, 452–464 (2005).
- Daneman, R., Zhou, L., Kebede, A. A. & Barres, B. A. Pericytes are required for blood–brain barrier integrity during embryogenesis. *Nature* **468**, 562–566 (2010).
- Carmeliet, P. & Jain, R. K. Molecular mechanisms and clinical applications of angiogenesis. *Nature* **473**, 298 (2011).
- Rafii, S., Butler, J. M. & Ding, B.-S. Angiocrine functions of organ-specific endothelial cells. *Nature* **529**, 316–325 (2016).
- Cheung, C., Bernardo, A. S., Trotter, M. W. B., Pedersen, R. A. & Sinha, S. Generation of human vascular smooth muscle subtypes provides insight into embryological origin-dependent disease susceptibility. *Nat. Biotechnol.* **30**, 165–173 (2012).
- Patsch, C. et al. Generation of vascular endothelial and smooth muscle cells from human pluripotent stem cells. *Nat. Cell Biol.* **17**, 994–1003 (2015).
- Loh, K. M. et al. Efficient endoderm induction from human pluripotent stem cells by logically directing signals controlling lineage bifurcations. *Cell Stem Cell* **14**, 237–252 (2014).
- Tanaka, M., Lyons, G. E. & Izumo, S. Expression of the Nkx3.1 homobox gene during pre and postnatal development. *Mech. Dev.* **85**, 179–182 (1999).
- Carson, J. A., Fillmore, R. A., Schwartz, R. J. & Zimmer, W. E. The smooth muscle γ -actin gene promoter is a molecular target for the mouse bagpipe homologue, mNkx3-1, and serum response factor. *J. Biol. Chem.* **275**, 39061–39072 (2000).
- Mack, C. P. Signaling mechanisms that regulate smooth muscle cell differentiation. *Arterioscler. Thromb. Biol.* **31**, 1495–1505 (2011).
- Sun, Q. et al. Myocardin-dependent activation of the CArG box-rich smooth muscle γ -actin gene. *J. Biol. Chem.* **284**, 32582–32590 (2009).
- Nishida, W. et al. A triad of serum response factor and the GATA and NK families governs the transcription of smooth and cardiac muscle genes*. *J. Biol. Chem.* **277**, 7308–7317 (2002).
- Yoshida, T. et al. Myocardin is a key regulator of CArG-dependent transcription of multiple smooth muscle marker genes. *Circ. Res.* **92**, 856–864 (2003).
- Song, S., Ewald, A. J., Stallcup, W., Werb, Z. & Bergers, G. PDGFR β + perivascular progenitor cells in tumours regulate pericyte differentiation and vascular survival. *Nat. Cell Biol.* **7**, 870–879 (2005).
- Rensen, S. S. M., Doevendans, P. A. F. M. & Eys, G. J. J. Mvan Regulation and characteristics of vascular smooth muscle cell phenotypic diversity. *Neth. Hear. J.* **15**, 100–108 (2007).
- Dorn, G. W. & Becker, M. W. Thromboxane A2 stimulated signal transduction in vascular smooth muscle. *J. Pharmacol. Exp. Ther.* **265**, 447–456 (1993).
- Low, E. L., Baker, A. H. & Bradshaw, A. C. TGF β , smooth muscle cells and coronary artery disease: a review. *Cell. Signal.* **53**, 90–101 (2019).
- Siekman, A. F. Biology of vascular mural cells. *Development* **150**, dev200271 (2023).
- Armulik, A., Abramsson, A. & Betsholtz, C. Endothelial/pericyte interactions. *Circ. Res.* **97**, 512–523 (2005).
- Folkman, J. & D'Amore, P. A. Blood vessel formation: what is its molecular basis? *Cell* **87**, 1153–1155 (1996).
- Orlova, V. V. et al. Functionality of endothelial cells and pericytes from human pluripotent stem cells demonstrated in cultured vascular plexus and zebrafish xenografts. *Arter. Thromb. Vasc. Biol.* **34**, 177–186 (2018).
- Bianco, P., Robey, P. G. & Simmons, P. J. Mesenchymal stem cells: revisiting history, concepts, and assays. *Cell Stem Cell* **2**, 313–319 (2008).
- Kim, H. et al. Pericytes contribute to pulmonary vascular remodeling via HIF2 α signaling. *EMBO Rep.* **25**, 616–645 (2024).
- Yuan, K. et al. Mural cell SDF1 signaling is associated with the pathogenesis of pulmonary arterial hypertension. *Am. J. Respir. Cell Mol. Biol.* **0**, 747–759 (2019).
- Ricard, N. et al. Increased pericyte coverage mediated by endothelial-derived fibroblast growth factor-2 and interleukin-6 is a source of smooth muscle-like cells in pulmonary hypertension. *Circulation* **129**, 1586–1597 (2014).
- Cao, Z. et al. Proteomic profiling of concurrently isolated primary microvascular endothelial cells, pericytes, and vascular smooth muscle cells from adult mouse heart. *Sci. Rep.* **12**, 8835 (2022).
- Tigges, U., Welsch-Alves, J. V., Boroujerdi, A. & Milner, R. A novel and simple method for culturing pericytes from mouse brain. *Microvasc. Res.* **84**, 74–80 (2012).
- Lendahl, U., Muhl, L. & Betsholtz, C. Identification, discrimination and heterogeneity of fibroblasts. *Nat. Commun.* **13**, 3409 (2022).
- Matsuda, M. et al. Recapitulating the human segmentation clock with pluripotent stem cells. *Nature* **580**, 124–129 (2020).
- Loh, K. M. et al. Mapping the pairwise choices leading from pluripotency to human bone, heart, and other mesoderm cell types. *Cell* **166**, 451–467 (2016).
- Owens, G. K., Kumar, M. S. & Wamhoff, B. R. Molecular regulation of vascular smooth muscle cell differentiation in development and disease. *Physiol. Rev.* **84**, 767–801 (2004).
- Beamish, J. A., He, P., Kottke-Marchant, K. & Marchant, R. E. Molecular regulation of contractile smooth muscle cell phenotype: implications for vascular tissue engineering. *Tissue Eng. B Rev.* **16**, 467–491 (2010).
- Consortium, T. S. et al. The Tabula Sapiens: a multiple-organ, single-cell transcriptomic atlas of humans. *Science* **376**, eabl4896 (2022).
- Roca, C. & Adams, R. H. Regulation of vascular morphogenesis by Notch signaling. *Gene Dev.* **21**, 2511–2524 (2007).

37. Jain, R. K. Molecular regulation of vessel maturation. *Nat. Med.* **9**, nm0603–nm0685 (2003).
38. Hoggatt, A. M. et al. The transcription factor Foxf1 binds to serum response factor and myocardin to regulate gene transcription in visceral smooth muscle cells. *J. Biol. Chem.* **288**, 28477–28487 (2013).
39. Ng, A. H. M. et al. A comprehensive library of human transcription factors for cell fate engineering. *Nat. Biotechnol.* **39**, 510–519 (2020).
40. Wang, G., Jacquet, L., Karamariti, E. & Xu, Q. Origin and differentiation of vascular smooth muscle cells. *J. Physiol.* **593**, 3013–3030 (2015).
41. Rajan, A. M., Ma, R. C., Kocha, K. M., Zhang, D. J. & Huang, P. Dual function of perivascular fibroblasts in vascular stabilization in zebrafish. *PLoS Genet* **16**, e1008800 (2020).
42. Ahuja, S. et al. The development of brain pericytes requires expression of the transcription factor nkx3.1 in intermediate precursors. *PLoS Biol.* **22**, e3002590 (2024).
43. Almalki, S. G. & Agrawal, D. K. Key transcription factors in the differentiation of mesenchymal stem cells. *Differentiation* **92**, 41–51 (2016).
44. Fernandopulle, M. S. et al. Transcription factor-mediated differentiation of human iPSCs into neurons. *Curr. Protoc. Cell Biol.* **79**, e51 (2018).
45. Skylar-Scott, M. A. et al. Orthogonally induced differentiation of stem cells for the programmatic patterning of vascularized organs and bioprinted tissues. *Nat. Biomed. Eng.* 1–14 <https://doi.org/10.1038/s41551-022-00856-8> (2022).
46. Loffredo, F. & Lee, R. T. Therapeutic vasculogenesis. *Circ. Res.* **103**, 128–130 (2008).
47. Wang, K., Lin, R.-Z. & Melero-Martin, J. M. Bioengineering human vascular networks: trends and directions in endothelial and perivascular cell sources. *Cell Mol. Life Sci.* **76**, 421–439 (2019).
48. Melero-Martin, J. M. et al. In vivo vasculogenic potential of human blood-derived endothelial progenitor cells. *Blood* **109**, 4761–4768 (2007).
49. Shepherd, B. R., Jay, S. M., Saltzman, M. W., Tellides, G. & Pober, J. S. Human aortic smooth muscle cells promote arteriole formation by coengrafted endothelial cells. *Tissue Eng. A* **15**, 165–173 (2009).
50. Maier, C. L., Shepherd, B. R., Yi, T. & Pober, J. S. Explant outgrowth, propagation and characterization of human pericytes. *Microcirculation* **17**, 367–380 (2010).
51. Chen, X. et al. Rapid anastomosis of endothelial progenitor cell-derived vessels with host vasculature is promoted by a high density of cotransplanted fibroblasts. *Tissue Eng. Pt A* **16**, 585–594 (2010).
52. Hendrickx, B. et al. Integration of blood outgrowth endothelial cells in dermal fibroblast sheets promotes full thickness wound healing. *Stem Cells* **28**, 1165–1177 (2010).
53. Lin, R.-Z., Moreno-Luna, R., Zhou, B., Pu, W. T. & Melero-Martin, J. M. Equal modulation of endothelial cell function by four distinct tissue-specific mesenchymal stem cells. *Angiogenesis* **15**, 443–455 (2012).
54. Melero-Martin, J. M. et al. Engineering robust and functional vascular networks in vivo with human adult and cord blood-derived progenitor cells. *Circ. Res.* **103**, 194–202 (2008).
55. Au, P., Tam, J., Fukumura, D. & Jain, R. K. Bone marrow-derived mesenchymal stem cells facilitate engineering of long-lasting functional vasculature. *Blood* **111**, 4551–4558 (2008).
56. Faal, T. et al. Induction of mesoderm and neural crest-derived pericytes from human pluripotent stem cells to study blood-brain barrier interactions. *Stem Cell Rep.* **12**, 451–460 (2019).
57. Xie, C.-Q. et al. A highly efficient method to differentiate smooth muscle cells from human embryonic stem cells. *Arter. Thromb. Vasc. Biol.* **27**, e311–e312 (2007).
58. Ferreira, L. S. et al. Vascular progenitor cells isolated from human embryonic stem cells give rise to endothelial and smooth muscle-like cells and form vascular networks in vivo. *Circ. Res.* **101**, 286–294 (2007).
59. Xie, C., Ritchie, R. P., Huang, H., Zhang, J. & Chen, Y. E. Smooth muscle cell differentiation in vitro. *Arterioscler. Thromb. Vasc. Biol.* **31**, 1485–1494 (2011).
60. Sumi, T., Tsuneyoshi, N., Nakatsuji, N. & Suemori, H. Defining early lineage specification of human embryonic stem cells by the orchestrated balance of canonical Wnt/ β -catenin, Activin/Nodal and BMP signaling. *Development* **135**, 2969–2979 (2008).
61. Kumar, A. et al. Specification and diversification of pericytes and smooth muscle cells from mesenchymoangioblasts. *Cell Rep.* **19**, 1902–1916 (2017).
62. Caplan, A. I. All MSCs are pericytes? *Cell Stem Cell* **3**, 229–230 (2008).
63. Crisan, M. et al. A perivascular origin for mesenchymal stem cells in multiple human organs. *Cell Stem Cell* **3**, 301–313 (2008).
64. Shen, M., Quertermous, T., Fischbein, M. P. & Wu, J. C. Generation of vascular smooth muscle cells from induced pluripotent stem cells: methods, applications, and considerations. *Circ. Res.* **128**, 670–686 (2021).
65. Caporarello, N. et al. Pericytes in microvessels: from “mural” function to brain and retina regeneration. *Int. J. Mol. Sci.* **20**, 6351 (2019).
66. Schlaeger, T. M. et al. A comparison of non-integrating reprogramming methods. *Nat. Biotechnol.* **33**, 58–63 (2015).
67. Wang, K. et al. Robust differentiation of human pluripotent stem cells into endothelial cells via temporal modulation of ETV2 with modified mRNA. *Sci. Adv.* **6**, eaba7606 (2020).
68. Lin, R.-Z. et al. Human endothelial colony-forming cells serve as trophic mediators for mesenchymal stem cell engraftment via paracrine signaling. *Proc. Natl. Acad. Sci. USA* **111**, 10137–10142 (2014).
69. Nowak-Sliwinska, P. et al. Consensus guidelines for the use and interpretation of angiogenesis assays. *Angiogenesis* **21**, 425–532 (2018).
70. Zheng, G. X. Y. et al. Massively parallel digital transcriptional profiling of single cells. *Nat. Commun.* **8**, 14049 (2017).
71. Consortium, I. H. G. S. et al. Initial sequencing and analysis of the human genome. *Nature* **409**, 860–921 (2001).
72. Hao, Y. et al. Integrated analysis of multimodal single-cell data. *Cell* **184**, 3573–3587.e29 (2021).
73. McGinnis, C. S., Murrow, L. M. & Gartner, Z. J. DoubletFinder: doublet detection in single-cell RNA sequencing data using artificial nearest neighbors. *Cell Syst.* **8**, 329–337.e4 (2019).
74. Cao, J. et al. The single-cell transcriptional landscape of mammalian organogenesis. *Nature* **566**, 496–502 (2019).
75. Hie, B., Bryson, B. & Berger, B. Efficient integration of heterogeneous single-cell transcriptomes using Scanorama. *Nat. Biotechnol.* **37**, 685–691 (2019).
76. Robinson, M. D., McCarthy, D. J. & Smyth, G. K. edgeR: a Bioconductor package for differential expression analysis of digital gene expression data. *Bioinformatics* **26**, 139–140 (2009).
77. Jin, S. et al. Inference and analysis of cell-cell communication using CellChat. *Nat. Commun.* **12**, 1088 (2021).
78. Morabito, S., Reese, F., Rahimzadeh, N., Miyoshi, E. & Swarup, V. hdWGCNA identifies co-expression networks in high-dimensional transcriptomics data. *Cell Rep. Methods* **3**, 100498 (2023).

Acknowledgements

Some illustrations were partially created with BioRender.com and released under a Creative Commons Attribution-NonCommercial-NoDerivatives 4.0 International license (<https://creativecommons.org/licenses/by-nc-nd/4.0/deed.en>). We thank Marco Corbo and Sheethal Umesh Nagalakshmi from MedGenome, Inc., for their assistance with the scRNA-seq analyses.

We thank Dr. George Church at Harvard University for kindly providing the NKX3.1 ORF. This work was supported by grants from the National Institutes of Health (R01HL151450 and R01HL128452 to J.M.M.-M.; R01GM125632, R01GM138407, R01HL148338, and R01HL133254 to K.C.) and the Beijing Natural Science Foundation (JQ23029 to K.W.).

Author contributions

U.L., K.W. and J.M.M.-M. conceived and designed the project. U.L., K.W., A.C.L., L.G., D.M.T., V.S.V., Y.K., X.W., R.-Z.L., M.C., M.M., and K.Y. performed the experimental work. Yadong.Z., performed single-cell transcriptional studies. Yadong.Z., Yonglin.Z., and K.C. performed bioinformatical analyses. All authors discussed and analyzed the data and edited the results. U.L. and J.M.M.-M. wrote the manuscript.

Competing interests

The authors declare no competing interests.

Additional information

Supplementary information The online version contains supplementary material available at <https://doi.org/10.1038/s41467-024-52678-8>.

Correspondence and requests for materials should be addressed to Kai Wang, Kaifu Chen or Juan M. Melero-Martin.

Peer review information *Nature Communications* thanks Kyle Loh, and the other, anonymous, reviewer(s) for their contribution to the peer review of this work. A peer review file is available.

Reprints and permissions information is available at <http://www.nature.com/reprints>

Publisher's note Springer Nature remains neutral with regard to jurisdictional claims in published maps and institutional affiliations.

Open Access This article is licensed under a Creative Commons Attribution-NonCommercial-NoDerivatives 4.0 International License, which permits any non-commercial use, sharing, distribution and reproduction in any medium or format, as long as you give appropriate credit to the original author(s) and the source, provide a link to the Creative Commons licence, and indicate if you modified the licensed material. You do not have permission under this licence to share adapted material derived from this article or parts of it. The images or other third party material in this article are included in the article's Creative Commons licence, unless indicated otherwise in a credit line to the material. If material is not included in the article's Creative Commons licence and your intended use is not permitted by statutory regulation or exceeds the permitted use, you will need to obtain permission directly from the copyright holder. To view a copy of this licence, visit <http://creativecommons.org/licenses/by-nc-nd/4.0/>.

© The Author(s) 2024